5-2018

Message in a Bottle: the Expression and Confirmation of ISF6_4831, a Polyethylene Terephthalate Hydrolase

Nathan A. Koconis
Winthrop University, nathankoconis@gmail.com

May 2018

To the Dean of the Graduate School:

We are submitting a thesis written by Nathan A. Koconis entitled Message in a Bottle: The Expression and Confirmation of ISF6_4831, a Polyethylene Terephthalate Hydrolase. We recommend acceptance in partial fulfillment of the requirements for the degree of Master of Science in Biology.

_____
Dr. Kristi Westover Ph.D., Thesis Advisor

_____
Dr. Nicholas Grossoehme Ph.D., Thesis Mentor

_____
Dr. Victoria Frost Ph.D., Committee Member

_____
Dr. Kathryn Kohl Ph.D., Committee Member

_____
Dr. Takita Sumter Ph.D., Interim Dean,
College of Arts and Sciences

_____
Dr. Jack DeRochi Ph.D., Dean,
Graduate School

MESSAGE IN A BOTTLE: THE EXPRESSION AND CONFIRMATION OF ISF6_4831, A POLYETHYLENE TEREPHTHALATE HYDROLASE

A Thesis

Presented to the Faculty

Of the

College of Arts and Sciences

In Partial Fulfillment

Of the

Requirements for the Degree

Of

Master of Science

In the Department of Biology

Winthrop University

May 2018

By

Nathan A. Koconis

Abstract

Polyethylene terephthalate (PET), the polyester used to make plastic bottles for soft drinks, is one of the top five sources of plastic waste in the world. Its abundance represents significant problems for municipalities and environments. Recycling PET polymers by traditional methods is possible, but success has been limited due to poor compliance, liability, cost, and other factors. Fortunately, a PET degradation pathway has been identified in *Ideonella sakaiensis.* Research on this pathway is still nascent and has not yet explored the PET hydrolase gene (ISF6_4831, or PETase) with its leading signal peptide intact. For this reason, the gene was transferred into *Escherichia coli* with subsequent expression and confirmation by PCR, SDS PAGE, Sanger sequencing, and Western blot. Apparent striking pink hues in the resultant growth media suggest that the secretion signal found in the gene is functional in *E. coli* and that the protein may hydrolyze some similar non-native substrates. This is noteworthy because it implies the potential for the gene moving laterally through environments rich in plastic waste without human intervention. We follow up by discussing some of the environmental and ecological implications of this and reviewing future directions for exploring this largely undocumented phenomenon.

Acknowledgements

I would like to thank my thesis mentor, Dr. Nicholas Grossoehme, for supporting this project, supplying the necessary lab materials, and guiding me through the unexpected minutiae of the research experience. I would also like to thank the chair of my committee, Dr. Kristi Westover, for providing boundless support and encouragement as it relates to the work that has been accomplished here. I would like to thank Dr. Victoria Frost for supplying ample advice in the context of microbiology and helping me infer meaning from our results, both expected and unexpected. I would also like to thank Dr. Kathryn Kohl for offering valuable insight on the DNA synthesis aspects of this project.

I would like to thank Carra Lyons, Hunter Sellers, Maddie Diaz, and Autumn Leggins as fellow members of the lab. Their experience with the equipment and reagents was instrumental to the success of this project. They also provided relevant fresh perspectives on interpreting results, helping me see angles I otherwise might have overlooked. I'd also like to thank the fellow graduate students in my department, especially Olivia Beasley, Joseph Horacek, Emily Powell, and Chris Garcia, whose varied perspectives helped me approach this project in the most unified way possible.

I would like to thank the Winthrop Research Council for funding this project, allowing me to work full-time on this endeavor over the Summer of 2017. Without this funding, it's quite likely the project could not have been completed. I'd like to thank the Biology department as a whole as well, for providing the academic support I needed through my thesis work and furnishing me with the skills necessary to grow as a scientist.

I would be remiss not to thank my closest friends, like Emily Thomas, Jessica Doscher, Anthony Sale, and family members like Sophie Koconis and Hannah Koconis. Without their compassion and support, I would not have been able to complete this project.

Table of Contents

List of Figures and Tables

Introduction

Plastic Waste

Plastic waste attracts global attention from governments, environmental groups and scientists; rightly so, since it poses a host of problems for the environment and society. Plastic's prized quality, its durability, makes it an unsustainable material. PET is a ubiquitous example. One of the most abundant polymers, PET plastic is water resistant and food safe, so it's most often used to make items like microwaveable meal trays, certain types of clothing, and soda bottles. Like most plastics, its resistance to corrosion and biodegradation means that it will likely continue to accumulate in the environment for decades. Some estimations even suggest that if plastic waste continues to accumulate unchecked, the mass of plastic in the ocean will exceed the mass of fish by the year 2050 (Jennings, et al., 2008; MacArthur, 2016).

It has been unequivocally shown that plastic waste upsets the balance of biotic and abiotic factors in any given ecosystem while simultaneously creating unique hazards that native wildlife is unequipped to deal with. Large pieces pose an entanglement risk, as seen with seals, dolphins, and turtles. Moderately-sized pieces pose an ingestion risk and have been found in the stomachs of albatross chicks, porpoises, planktivorous fishes, mesopelagic fishes, whales (Sigler, 2014), and even vultures (Auge, 2017). Microplastic particles are the most serious risk to the environment and pose the greatest challenge in terms of cleanup. Microplastic particles have been shown to inhibit algae growth inversely proportional to their size (Zhang, 2017), implying that the smallest particles produce the most far-reaching effects on the environment. The trophic effects seen with microplastics are amplified as well, affecting behavior, growth, reproductive systems, and mortality rates

Figure I1: Lepas ansifera barnacles growing on some PET plastic (Whitehead et al., 2011).

across species (Chae, 2017). Humans are not exempt from these effects, trophic or otherwise. Microplastic particles have been detected in atmospheric fallout in Paris, suggesting that residents must be breathing these materials constantly. These synthetic particles and fibers have been found in lung biopsies and have been associated with inflammation, dyspnea, and increased risk for disease, especially in susceptible individuals (Prata, 2018). Even designated green facilities aren't cleanly disposing of plastics. For example, higher rates of eczema, esophageal irritation, mucocutaneous symptoms, and respiratory symptoms have been reported near recycling facilities in Japan, most likely due to the elevated levels of volatile organic compounds (VOCs) found in the air nearby (Xin, 2018).

While plastic has negatively impacted some species, it has positively impacted others. Studies in South Africa showed rubber sandals and plastic debris (including PET) act as substrata to various species of barnacles (See Fig. I1). The abundance of colonizing sites leads to an abundance of barnacles, throwing ecosystems out of balance (Whitehead, 2011). Some hermit crabs and other creatures have even been seen actively seeking litter for use as shells (See Figure I2) (Barreiros, 2009). All of these findings point to the asymmetrical effects of plastic waste on environments as an anthropogenic force that fundamentally alters the balance of ecosystems across the world while endangering human health.

Current Recycling Trends

Although industrial processes for recycling plastic have been in place for decades, recycling rates in many developed countries rarely exceed 60%. The United States has a worse record, averaging less than 30% in 2010 (Zhang, 2013). Production of PET is increasing every year and is expected to reach nearly 20 million metric tons globally by the end of the year 2018. However, considering the poor recycling practices of the US, it's also expected that in the same year, 1.5 million tons will be discarded in this country alone (MacArthur, 2016).

Figure I2: This hermit crab has an indigestible bottlecap "shell" that is stronger and lighter than a natural one (Barreiros, 2009).

In the United States, the dominant recycling paradigm for PET entails exporting the plastic waste to China (or occasionally Taiwan or Singapore), where it's cleaned, melted, and made into non-food items, like clothing or carpeting. These products are then sold back to the United States. This round-trip shipping process is quite wasteful, potentially offsetting the environmental benefits of the recycling in the first place. Of the PET scrap that remains in the US, many mixed media products aren't recycled because it isn't economically feasible to justify the process of collecting them and separating out the PET. Examples include construction products, packaging, motor vehicles, and the clothing and carpeting products that China makes from PET scrap. Furthermore, experts estimate that only half of the PET collected for recycling is ever

actually reused. Accounting for all this, that sets the US PET recycling rate at roughly 12% (Forrest, 2016; See Figure I3).

Even if the recycling rate were much higher, that wouldn't solve the main issue with PET recycling. Separating the PET plastic bottle from its label, its cap, and the food particles inevitably stuck to it is a difficult and expensive process (Forrest, 2016). That's why so-called bottle-to-bottle recycling, producing 100% post-consumer PET plastic bottles, has still not been perfected at a competitive cost. It's difficult and expensive to completely clean previous contaminants from the plastic and/or degrade the materials for remolding. This poses a liability for dietary, religious, and allergenic reasons. In considering the energy costs of bottle-to-bottle recycling, it has always been industrially cheaper to make new plastic bottles. No recycling process has ever been clean, efficient, and cheap enough to satisfy demand thus far (Welle, 2011). There have been some

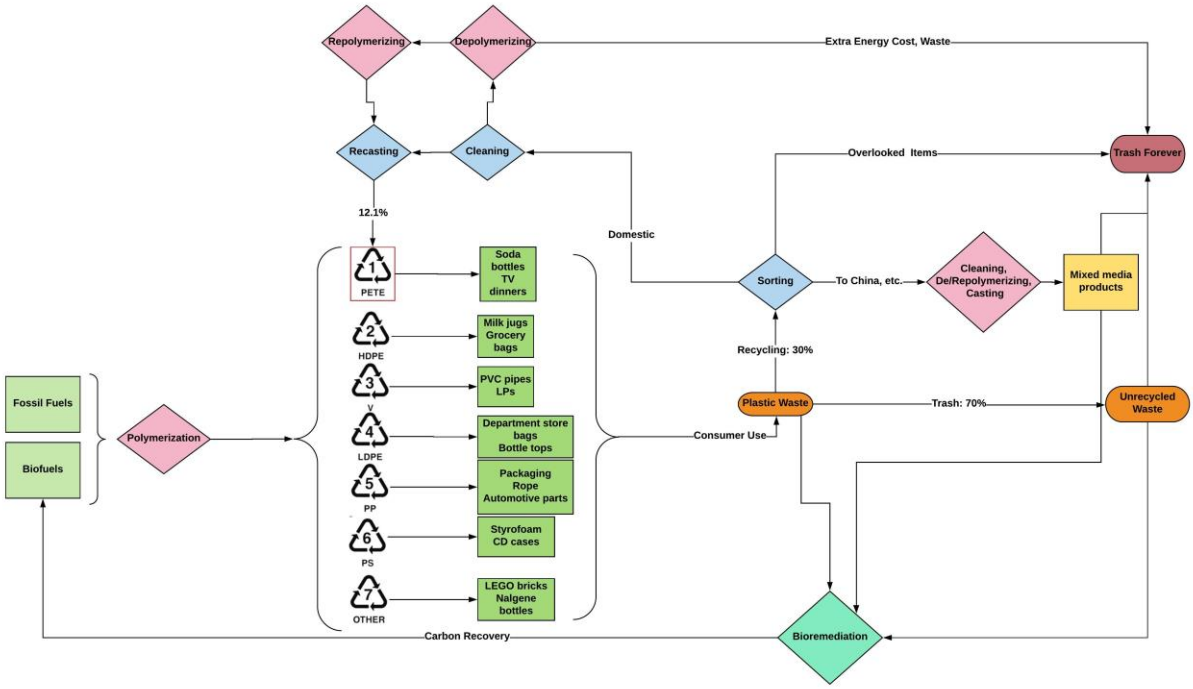

Figure I3: Flow model of plastic recycling in the United States. PET is highlighted in red. Only 12.1% of PET waste is recycled and reused in the US. The rest is either exported and made into mixed media products or sent to landfills. Current PET recycling processes either require a so-called supercleaning step, a de/repolymerization step, or both. Decisions for which process to use depend on the goal product for the 100% recycled PET (rPET). If it is intended to be used as a 100% rPET bottle or food container, a supercleaning step is necessary to remove any potential allergens or pathogens from previous use. This can be expensive and time-consuming. De/repolymerization can replace this, but the chemical reactions involved require specialized reagents and generate toxic waste (Forrest, 2016).

government initiatives in Europe to offset that cost, but the economic burden is always contingent on the relative prices of oil (to make new plastic) and energy (to recycle old plastic) (Forrest, 2016).

PETase

However, modern bioprospecting findings suggest that enzymes found in nature can be adapted to human needs. In March of 2016, a bacterium that uses PET plastic as its sole food source was discovered in Sakai, Osaka, Japan. This creature, dubbed *Ideonella. sakaiensis,* possesses two enzymes that form a biochemical pathway for the catabolism of

PET plastic, similar to those seen by filamentous fungi, such as *Fusarium oxysporum* (Yoshida et al., 2016). Digestion of the plastic is a three-step process. First, PET hydrolase (*ISF6_4831*) catalyzes the hydrolysis of the ester linkage between terephthalate monomers producing mono (2-hydroxyethyl) terephthalate (MHET). The second enzyme, MHET hydrolase (*ISF6_0224*), catalyzes a second ester hydrolysis to generate terephthalic acid (TPA) and ethylene glycol; notably, these are the typical reagents used for industrial PET synthesis (See Figure I4). Last, TPA is oxidized by TPA 1,2-dioxygenase, the entry point

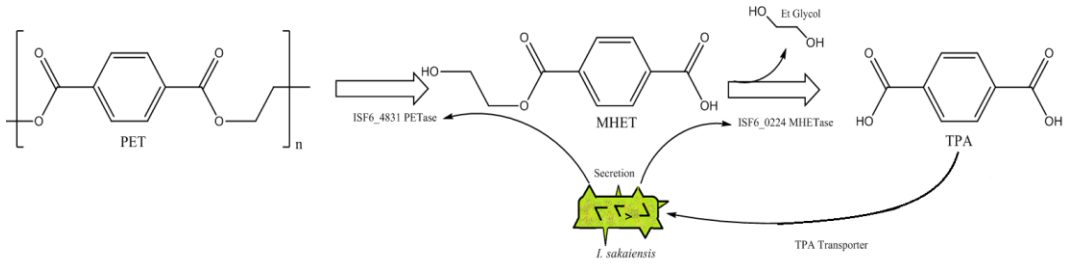

Figure I4: *I. sakaiensis* uses its appendages to secrete PETase where the plastic touches its environment. PET is degraded into MHET, which is degraded into TPA and ethylene glycol by MHETase. Uptake of TPA occurs via TPA transporter. TPA is then oxidized by TPA 1,2-deoxygenase (Yoshida, et al., 2016).

for the PCA 4.5 cleavage pathway, which fully oxidizes the compound for energy production. This process eventually culminates in full catabolism and the release of waste products such as CO_2 (Yoshida et al., 2016).

In its native context, this PETase is quite remarkable, not only for what it does, but for where it acts. PET (like all plastics) is a polymer, too large to be endocytosed natively. Uptake of polymeric materials to be digested cannot occur before they're broken into monomers. For this reason, the bacteria must secrete the PETase from specialized cell appendages (See Figure I4). Secretion of the protein is coded by a signal peptide on the N-terminus (Yoshida, et al., 2016). PET is practically insoluble, (GESTIS Substance Database, 2007), so this degradation can only take place at junctions where water touches

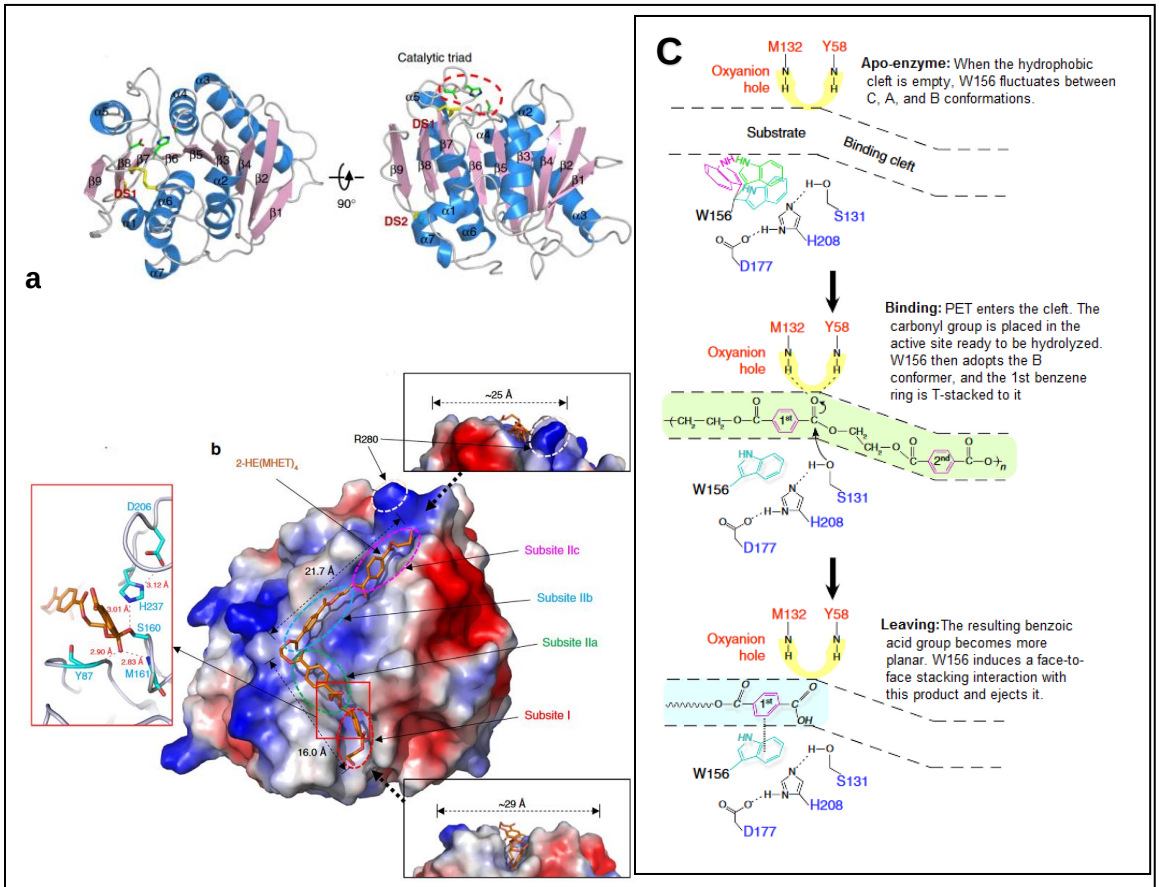

Figure I5: Models of the PETase protein as confirmed by crystallography. **a**: The protein is stabilized by antiparallel beta sheets and two disulfide bonds. Removing the bridge closest to the catalytic triad severely impacts PETase function, suggesting that its structural role is key to PETase's activity. The catalytic triad can also be clearly seen here (Han, 2017). **b**: Space filling model of PETase. Residue numbers are shifted upward due to carrier plasmid expression. The hydrophobic landing site can be clearly seen, able to accommodate 4 monomers. The dividing line between subsites I and II is the cleavage point, indicated by the red box (Joo, 2018). **c**: W156 adopts varying conformers to help move substrate in and product out. This is only possible due to the Ser present at 185. This would typically be a His in homologous enzymes. Numbering here matches numbering seen in **a** (Han, 2017).

the plastic, not freely dissolved in the media itself. This topographical feat is achieved by the positioning of a hydrophobic cleft on the PETase, acting as a landing site for the plastic. This cleft can be divided into two main subsites, I and II, delineated along the cleavage site. Subsite II can further be divided into IIa, IIb, and IIc, where up to three successive repetitions of the PET monomer (or similar substrate) may align. Near the active site, W156 fluctuates through various conformations, facilitating to position the polymer for hydrolysis and subsequently eject it after the reaction is completed. In other words, W156

acts as a spatula that flops around to move PET in and MHET out. Hydrolysis is performed with a typical catalytic triad (S131-H208-D177). Serine serves as the nucleophile, polarized by histidine, which is stabilized by aspartic acid. This has all been confirmed by crystallography. Other PETases exhibit similar hydrolytic mechanisms but differ in their ability to shuttle PET to the active site because they have a Trp locked in the "C" conformation. This offers a potential explanation for ISF6_4831's faster performance than previously discovered enzymes (Han, 2017). However, a subsequent study suggested that the presence of a second disulfide bond and a uniquely tuned subsite II PETase activity. Subsite II was hypothesized to be adaptive primarily because it can hold three linked monomers, the subsequent pieces of the PETase to be hydrolyzed, while the leading edge of the molecule is being cleaved. This was corroborated by site-directed mutagenesis of the edge of subsite IIc to be less bulky and more hydrophobic (R→A), increasing PETase activity (Joo, 2018). This degradation mechanism represents an instance of an organism that lives in water but degrades an insoluble object. Breakdown into MHET renders the plastic partially soluble (predicted value: 27.3 g/L) (US EPA, 2018) and produces a more bite-sized molecule for further degradation into TPA. Uptake of TPA occurs via TPA transporter (Yoshida et al., 2016; see Figure I4 and I5).

Notably, ISF6_4831 PETase has been shown to target non-native substrates and produce chromophores. Although it targets PET (Yoshida, et al., 2016) with greater specificity than any of its homologous enzymes, para-nitrophenyl phosphate (PNPP) assays have been used in previous studies to roughly gauge enzymatic activity, using direct spectrophotometric analysis for quantification (Han, 2017). The enzyme has also shown activity on bis(2-hydroxyethyl) terephthalic acid (BHET), an inert monomer of PET

(Yoshida, et al., 2016). This suggests the presence of other hitherto undiscovered organic compounds with ester bonds that may be targeted by PETase, especially if they have aromatic rings.

Objectives

There has been very little research on this enzyme. At time of this project's inception, only a single study had ever been published on it. There are now three, not counting this project. No two papers agree on an ideal method for expression and purification of this protein. Exploring the different options for expression in various *Escherichia coli* strains will provide context as to which options are best. This will also be done for different growing conditions, induction concentrations, media, expression plasmids, and purification methods.

PET, like nearly all plastics, is mostly hydrocarbons, and as such is an energy-dense material. For this reason, *I. sakaiensis'* potential as a pollution-processing organism is limited by its own metabolism (Yoshida et al., 2016). Put simply, plastic is very filling, and it isn't hungry enough to eat plastic waste faster than industry produces it. Therefore, the goal of this project was to transform expression strains of *E. coli* with the ISF6_4831 gene to explore the possibility of a scalable biochemical system for degrading PET plastics in industry and in damaged environments. Cloning the PET hydrolase gene from *I. sakaiensis* into *E. coli* may allow the purification of large quantities of a stable and functional form of the enzyme.

Additionally, the conserved nature of the signal peptide suggests that it should function in other gram-negative bacteria, including *E. coli* (Juncker, 2003). However, this

has not been studied by any of the previous papers. *E. coli* does not have the periplasmic extensions seen in *I. sakaiensis* (Yoshida et al., 2013), so it's possible the secretion signal may be inactive. It may also signal for the protein to be shuttled to the periplasmic space or even packaged into inclusion bodies if the sequence appears too xenobiological. If it works, however, it would be the first time anyone has documented this enzyme being secreted by a non-native organism. It could even provide a foundation for industry, in which a dynamic culture medium would be used to clean and purify plastic bottles for recycling, without any enzyme purification steps required. It could also be used for environmental cleanup in this way. Furthermore, confirming that the signal peptide is functional in non-native organisms would imply possibility for transfer of that pathway across species. Therefore, using the full gene with its signal sequence will also inform potential for PETase (and genes like it) to proliferate through environments via horizontal gene transfer and otherwise.

Materials and Methods

Cell Strains

DH5α *E. coli* cell strains were used for storing the plasmid DNA. These cells are best suited to hold DNA because they don't use heterologous recombination to repair broken DNA. They're also engineered to have fewer endonucleases, which makes transforming easier. They're also phage resistant and can be used to perform blue/white screening using β-galactosidase. This is consistent with typical methods (New England Biolabs; 5-alpha manual).

Expression strains used were BL21, Rosetta, and NiCo. Using three different strains of *E. coli* is allows for best-case (and worst-case) scenarios when expressing and purifying.

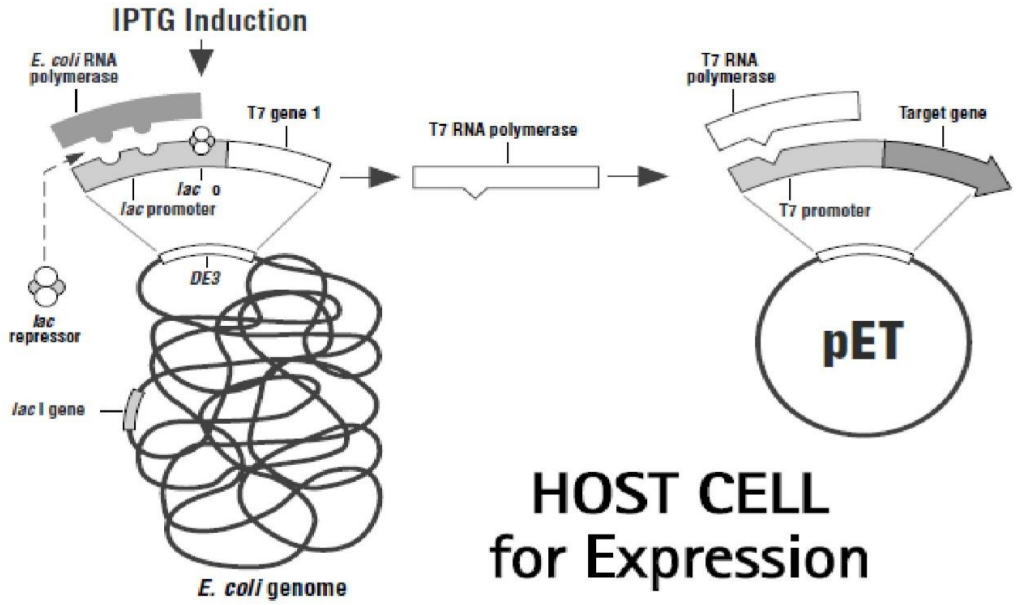

Figure M1: IPTG Induction allows the production of a T7 RNA polymerase. This polymerase then strongly binds to the pET plasmid and produces the target gene. This allows for inducible, precise control of expression (Novagen, Competent Cells Manual, 2016).

The first, a generic BL21 strain, is the standard strain for protein expression. It requires the presence of an IPTG inducer molecule to activate a lac operon which codes for expression

of a T7 viral RNA polymerase. This is the only way the *E. coli* can make this polymerase. The ISF6_4831 gene will be controlled by a T7 promoter. Therefore, the addition of IPTG to the cell solution allows expression of the gene. This affords precise control over protein expression (See Figure M1). Also, unlike DH5α cells, the BL21 cells are engineered to be deficient in certain proteases to maximize the amount of protein produced. They are not entirely protease-free, but they produce far fewer proteases than DH5α cells (Novagen pET system manual, and New England Biolab BL21 datasheet). Both other strains are fundamentally considered BL21 strains, but with other added properties. The Rosetta strain has more copies of esoteric tRNAs, which effectively accounts for codon biases in xenogenic mRNA. Since the gene was codon-optimized, it's not likely that would have been an issue though (See Novagen Rosetta Datasheet). The NiCo competent strain is designed to optimize purification. It contains significant genome deletions to remove nickel and cobalt (hence the name NiCo) ions. This allows easier purification of the His-tagged protein later on after expression (See Papaneophytou and Kontopidis, 2013; see also New England Biolab NiCo Datasheet). Competent cells were made according to the $CaCl_2$ protocol as described by Chan et al. (2013).

Cloning Procedures

The PETase gene was derived from the protein sequence and codon-optimized as described by Yoshida et al. (2016) with the exception that the signal peptide was included

PETase Sequence - optimized for *E. coli*
Text Map

```
           10        20        30        40        50
       *    *    *    *    *    *    *    *    *    *
     1 ATGAATTTTCCGCGTGCTTCCCGCTTAATGCAAGCCGCGGTACTGGGCGG 50

           60        70        80        90        100
       *    *    *    *    *    *    *    *    *    *
    51 TTTGATGGCGGTAAGTGCCGCTGCAACAGCGCAGACCAACCCGTATGCCC 100

           110       120       130       140       150
       *    *    *    *    *    *    *    *    *    *
   101 GTGGTCCCAATCCGACCGCAGCTTCTCTGGAAGCCTCAGCTGGCCCGTTT 150

           160       170       180       190       200
       *    *    *    *    *    *    *    *    *    *
   151 ACTGTGCGCTCATTCACGGTTAGTCGTCCTTCAGGCTATGGTGCAGGCAC 200

           210       220       230       240       250
       *    *    *    *    *    *    *    *    *    *
   201 CGTCTACTATCCGACGAATGCAGGCGGAACGGTAGGAGCGATCGCGATTG 250

           260       270       280       290       300
       *    *    *    *    *    *    *    *    *    *
   251 TGCCGGGTTATACTGCACGCCAGAGCTCGATCAAATGGTGGGGTCCACGG 300

           310       320       330       340       350
       *    *    *    *    *    *    *    *    *    *
   301 TTAGCGTCCCATGGCTTCGTCGTGATTACCATCGACACCAACAGCACACT 350

           360       370       380       390       400
       *    *    *    *    *    *    *    *    *    *
   351 GGATCAGCCCTCATCTCGCAGCTCTCAGCAGATGGCTGCCCTCCGTCAGG 400

           410       420       430       440       450
       *    *    *    *    *    *    *    *    *    *
   401 TCGCCAGCCTGAACGGGACAAGCAGCTCTCCGATTTACGGCAAGGTTGAT 450

           460       470       480       490       500
       *    *    *    *    *    *    *    *    *    *
   451 ACGGCCCGTATGGGCGTTATGGGGTGGTCCATGGGTGGTGGTGGTTCGCT 500

           510       520       530       540       550
       *    *    *    *    *    *    *    *    *    *
   501 GATTAGTGCTGCAAACAATCCGAGTTTGAAAGCAGCCGCACCTCAAGCGC 550

           560       570       580       590       600
       *    *    *    *    *    *    *    *    *    *
   551 CTTGGGATAGCTCAACGAACTTTAGCAGCGTCACTGTGCCAACCCTGATC 600

           610       620       630       640       650
       *    *    *    *    *    *    *    *    *    *
   601 TTTGCGTGCGAAAACGACTCGATTGCGCCAGTGAACTCCAGCGCGCTTCC 650

           660       670       680       690       700
       *    *    *    *    *    *    *    *    *    *
   651 GATCTACGATTCGATGAGTCGCAATGCCAAACAGTTCCTGGAGATTAATG 700

           710       720       730       740       750
       *    *    *    *    *    *    *    *    *    *
   701 GCGGGAGTCACTCGTGTGCGAATTCTGGAAACTCTAACCAAGCGCTGATT 750

           760       770       780       790       800
       *    *    *    *    *    *    *    *    *    *
   751 GGCAAGAAAGGGGTTGCGTGGATGAAACGGTTCATGGACAACGATACCCG 800

           810       820       830       840       850
       *    *    *    *    *    *    *    *    *    *
   801 CTATTCCACCTTTGCCTGTGAAAACCCGAATTCCACCCGCGTGAGCGATT 850

           860       870
       *    *    *    *
   851 TTCGCACGGCGAATTGCTCG 870
```

Figure M2: The codon-optimized PETase gene. The signal sequence is highlighted.

in the sequence (See Figure M2). PCR primers were then designed to add Nde1 and BamH1 endonuclease sites to the 5' and 3' edges of the gene respectively. Nde1 and BamH1 restriction borders allow for easy unidirectional insertion into a plasmid with corresponding sites. These borders allow palindromic cleavage at the A-T sites of the Nde1 border and the G-G sites at the BamH1 border using their eponymous restrictase enzymes. This creates a "sticky" non-reversible linear DNA strand that can be inserted into any compatible plasmid that has also been treated with Nde1 and BamH1 (See Hwang et al., 2003; and

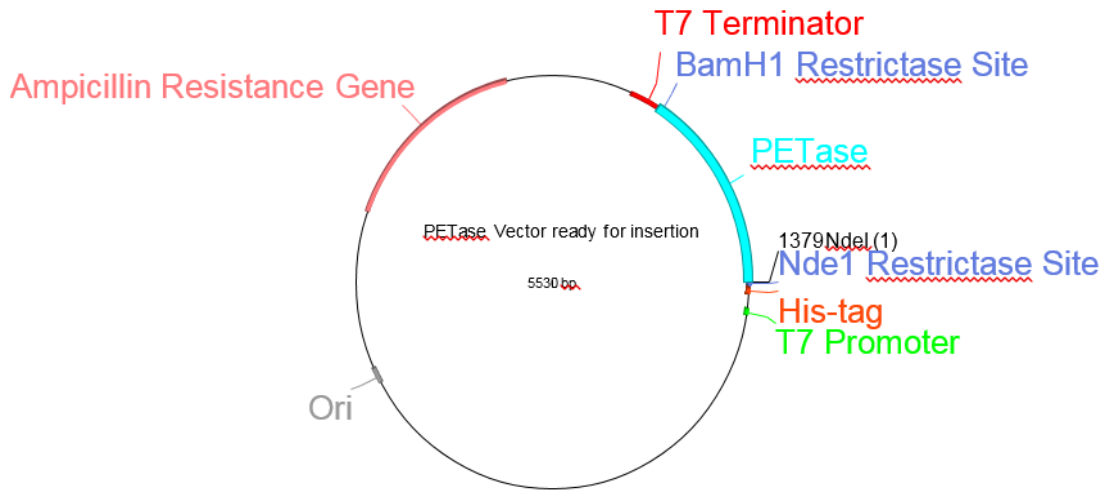

Figure M3: The pET14-b plasmid with PETase insert and Ampicillin Resistance. This construct was inserted into *E. coli* by heat shock treatment (Visualization made with ApE; see Davis, 2013).

New England Biolabs Restriction Endonuclease Manual). Strand insertion must then be completed with a DNA ligase to anneal the strand in place and restore the plasmid to its circular shape (See Figure M3 for completed pET14 example, and Novagen pET-14b vector map). Actual plasmid insertion can be done a variety of ways, but the most convenient method is heat-shocking the *E. coli* in hypertonic solution, encouraging absorption of the plasmid from their surroundings (Hwang et al., 2003; see also New England Biolab NiCo and BL21 manuals). To remove the signal sequence an alternative PETaseDelNde1 primer was designed to amplify the gene excluding the first 81 nucleotides (Yoshida et al., 2016).

The commercially available pET3, pET14, pET15, and pET28 plasmids were chosen as insertion vectors because they have Nde1-BamH1 restriction sites. Each plasmid also has an antibiotic-resistance gene. In the case of pET3, pET14, and pET15, the plasmid confers resistance to ampicillin. PET28 confers resistance to kanamycin. PET14, pET15, and pET28 plasmids also have hexa-histidine sequences for purification and identification of the resultant protein. The pET14 and pET15 plasmids place a His-tag on the N-terminus

and the pET28 plasmid places a His-tag on both the N- and C-termini. Subsequently plating the cells on antibiotic media selects for the *E. coli* that have received the gene. This is standard practice (Chen, 2011).

Transformation Protocols were performed as described in NEB DH5α manual, with the exception that a 1:9 ratio of 10% dextrose solution to LB media was used in place of SOC (New England Biolabs, High Efficiency Transformation Protocol; 2016). After plating the cells on antibiotic media, promising colonies were cultured in antibiotic LB and T7 PCR was used to detect the size of the insert directly from culture (Yoshida et al., 2016). If PCRs from culture showed an insert of correct size, plasmid DNA was harvested from cultures using an IBI DNA miniprep kit, according to company protocol (2018) with the exception that autoclaved water was used instead of elution buffer. Cell stocks were also made from promising cultures with a ratio of 1:1 50% glycerol stock to cultured cells. These stocks were made in airtight 1.5 mL microcentrifuge tubes and stored at -80°C (Chan et al., 2013).

Sanger sequencing was done using T7 primers. For the pET3 plasmid, sequencing was done on samples of whole plasmid. For the pET14 and pET28 plasmids, sequencing was done from cleaned T7 PCR amplification results run in lab (Eurofins Genomics, 2017). PCR amplification results were cleaned using column filtrations as per IBI Scientific (2018) manual, with the exception that deionized water was used instead of elution buffer. Post-confirmation of DH5α stocks containing an insert of correct size and sequence, transformation of expression strains followed, followed by a further screening step using antibiotic media and creation of a cell stock (IBI Scientific, 2018).

Protein Purification

Expression was performed as described by Yoshida et al., except that conditions where the cells were induced for 1-2 hours instead of overnight received 1.0mM IPTG instead of 0.1mM as in the overnight conditions (2016). Induction proceeded, and cells were centrifuged to a pellet. Supernatants were collected for analysis and cell pellets were suspended in lysis buffer. Buffers were made as described by Yoshida et al., (2016) with the exception that no imidazole was added to the main lysis buffer. For ion-exchange purification, wash buffer was 50mM TRIS HCl, 100 mM NaCl, pH=8.0; elution buffer was 50mM TRIS HCl, 1M NaCl, pH=8.0. Cells were lysed by sonication, according to a 10'' on 45'' off cycle at 4 °C. PMSF was added to prevent degradation of the expressed protein (Gold, 1967).

Lysates were centrifuged, and the resultant inclusion bodies were collected. Lysates were filtered using fast protein liquid chromatography (FPLC). SP ion-affinity columns, Q ion-affinity columns, and Nickel-affinity columns were used according to protocols as described by their manufacturers (USB Corporation). Ion-affinity columns work by binding the charged peptide bonds of proteins as they filter through. After running the lysate through the column and rinsing it with a neutral buffer, the sample is eluted by washing with a salt solution or a pH gradient. The premise is that the ions present have a greater affinity for the ion column than the protein. Nickel columns use a similar principle. The nickel ions in the resin of the filter prefer to bond to the hexahistidine tag mentioned previously. After rinsing with a neutral buffer, the protein is eluted with an imidazole buffer

(Sigma-Aldrich, 2018; GE Healthcare Life Sciences, 2018). As the column loading, filtration, and elution proceeds, the FPLC readout uses absorbance spectra to predict the amount of protein eluted from the column in a given, labeled fraction (Agilent Technologies). Large peaks on absorbance spectra correspond to large amounts of protein eluted. Fractions containing peaks like these were the fractions of interest for analysis by Sodium dodecyl sulfate-polyacrylamide gel electrophoresis (SDS PAGE) (Yoshida et al. 2016; see also Grossoehme Purification Methods, 2016).

SDS PAGE was used to determine the size of the protein of interest. Proteins were visualized by Coomassie staining (Bio-Rad). The ladders used were New England Biolabs Unstained 10-250 kDa protein ladder (ID:P7703), Color Prestained Broad Range (ID:P7712S), and Protein Marker Broad Range 2-212 kDa (ID:P7702) (2018) (See Figure M4). The expected size of the protein is between 30 and 34 kDa (Yoshida et al., 2016).

Experimental Schedule

Primers and the PETase sequence were ordered from Eurofins Genomics (2018; see supplementary data, Table S1). The PETase gene was amplified by PCR from its carrier plasmid. In the process, Nde1 and BAMH1 sites were added. Concurrently, a request was sent to Phyre2 (2015) to generate a potential model for the PETase enzyme. Molecular graphics images were produced using the UCSF Chimera package from the Resource for Biocomputing, Visualization, and Informatics at the University of California, San Francisco (supported by NIH P41 RR-01081). Chimera was used to analyze and label the predictive model (Pettersen, 2004). The following Summer, the PETase gene, pET3, and pET14 were digested by Nde1 and BamH1 endonucleases. The results were cleaned and size-purified by agarose gel electrophoresis. The results were cleaned again and the complimentary "sticky" pieces were ligated according to standard protocols for T4 ligase. Sometimes, so-called "quick" ligases were used, but they never succeeded (Chen, 2011). Ligation results were transformed into DH5α and screened by PCR. Promising colonies were sequenced. The construct was extracted from DH5α and

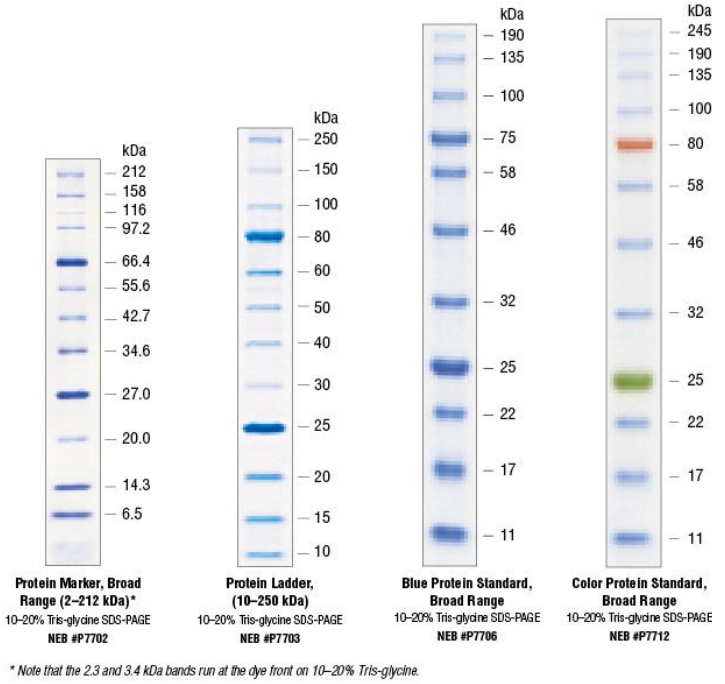

Figure M4: Protein Standards used to determine molecular weight by SDS PAGE analysis (New England Biolabs, 2018).

cloned into expression strains. This was followed by analysis by SDS PAGE. Subsequently, cell stocks for pET14 and pET3 PETases had been successfully generated from BL21 cells, Rosettas, and NiCos. The pET14 insert seemed correct according to PCR amplification and subsequent size analysis by gel electrophoresis, but it required a T7 PCR sample sent directly to be sequenced to get intelligible data. The fidelity of the pET14 insert was confirmed in October 2017. In light of this, a Western Blot was run in October on key FPLC fractions of interest. The Western Blot uses immunohistochemistry to detect the presence of the protein by sticking to the His-tag. The following primary antibody was used in this experiment: 6x-His Tag Monoclonal Antibody (mouse IgG) from GeneTex, catalog # GTX15149. It was diluted to 1x fold in TBST with 0.05g/mL nonfat dry milk as a blocking agent. The following secondary antibody was used in this experiment: Goat anti-Mouse IgG Secondary Antibody, AP from GeneTex, catalog # GTX213111-04 (GeneTex, 2013). It was diluted to 1x in TBST with 0.5x diluted StrepTactin-AP conjugate for visualization. SDS PAGE gel results were transferred to plyvinyldifluoride (PVDF) membranes at 15 volts for 15 minutes. The resultant membrane was incubated with primary antibody overnight. The next day, the membrane was washed with TBST and incubated with the second antibody. The membrane was then washed and visualized (GeneTex, 2013).

Expression and purification success was low/unconfirmed, so construction of a pET28 PETase began in November 2017. It was transformed into DH5α cells on January 2018. Sequencing was completed in March 2018. Comparison of PETase$^{(+)}$ and PETase$^{(-)}$ pET28 cells was done in March as well. pET21 PETase DH5α cells were also made, but

the time constraints of this project meant that sequencing was not possible. Photographs of pink colours were taken after lysis step and as a post-research survey on all stored samples.

Construction of a signal-free PETase was completed in March 2018. This construct was cloned into DH5α cells on the same month, and expression and lysis were completed shortly after.

Results

Cloning Confirmations

T7 PCR screening of DH5α pET3a PETase and pET14b PETase colonies showed specific inserts of the expected size. Colonies of interest were labeled and cultured. Plasmid DNA extracted from these cultures was screened a second time in tandem with a double-digest using Nde1 and BamH1 endonucleases. This reconfirmed the size of the inserts

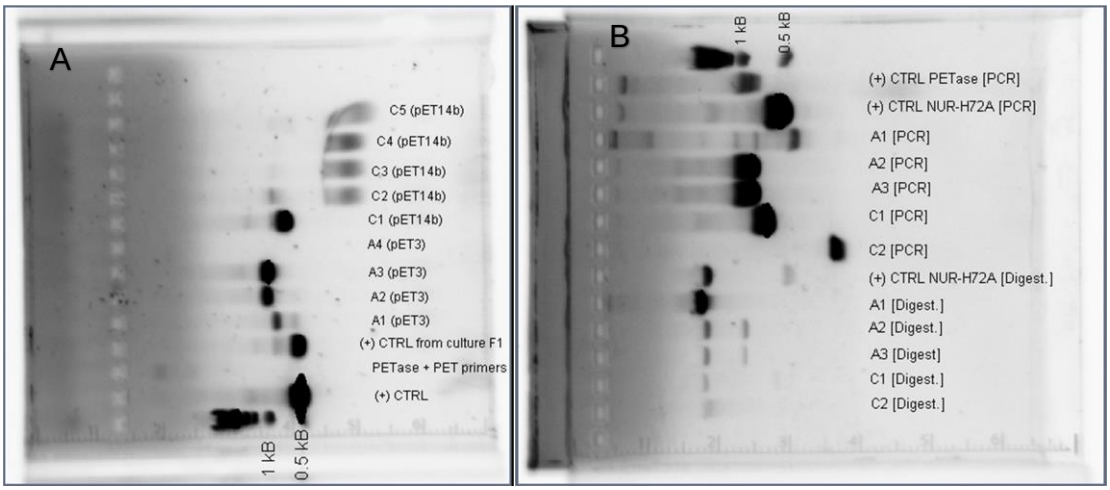

Figure R1: Condition A was pET3 and condition C was pET14. **A**: PCR Screenings of DH5α cells after transformation but before purification and extraction of DNA. PCRs done with T7 primers. The control PCR gene (NUR) is a 500-base sequence. **B**: Promising colonies were cultured overnight. Plasmids were extracted and purified, and reconfirmation of PCR was done. Digestion using Nde1-BamH1 sites showed the sequence liberated from its carrier plasmid. The control sequence is the same as A.

while rejecting previous false positives found from testing the colonies directly. Inserts found were consistent with the expected size of the PETase gene (~800 bp), plus the edges of the plasmid amplified by the T7 primers (~200 bp) (See Figure R1). Attempted ligations and transformations continued until DH5α stocks of the pET14b were confirmed by PCR screening (See Figure R2). Similar confirmations were done with the pET28 PETase, showing inserts of the expected size. Compared with the pET14 PETase, the pET28

insertion is slightly larger (See Figure R3). pET21 PETase screening is also shown. Two

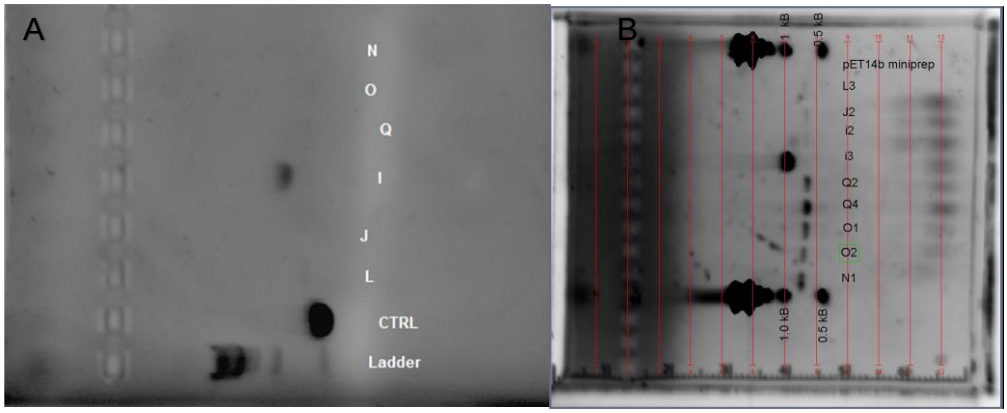

Figure R2: Conditions I-Q were more pET14 ligation/transformation attempts. **A**: PCR screening of pET14 DH5α cells after transformation and culturing, before purification and extraction. Control sequence is NUR, a ~500 bp sequence for context **B**: Promising colonies were cultured overnight. Plasmids were extracted and purified and reconfirmation of PCR was done. The control sequence is the same as A.

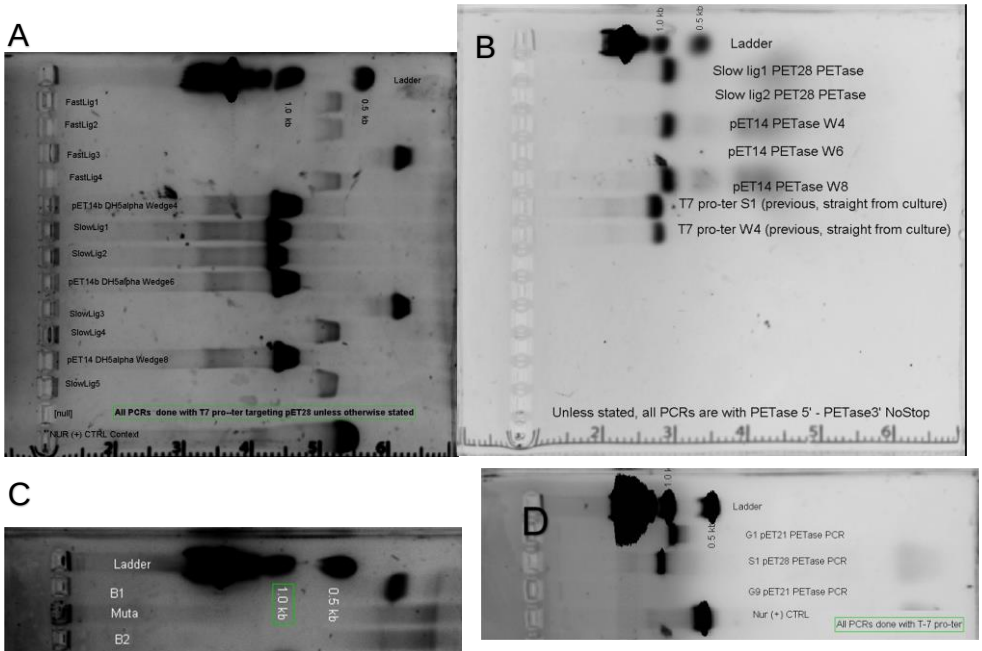

Figure R3: **A**: PCR screenings of DH5α pET14b (as control) and pET38 ligations (some using "slow" T4, other attempts with "fast" ligase). 1 and 2 show inserts of the expected size. In this case, inserts are slightly larger than pET14 ones because they have His-tags on both sides as a result of the 3' NoStop primer introduced in PCR. **B**: Screenings of same cell stocks after purification of plasmid DNA. Screenings of pET14 from A are used as controls in B. B uses PETase primers. The slightly reduced weight of the resultant band is an expected effect of this. **C**: Screenings of the same strain for pET21 PETase inserts. Two colonies show expected size. **D**: Confirmation from cultures of two promising colonies. Band is of expected size, just over 1 kb.

colonies had an insert of the expected size and were selected for reconfirmation by PCR. Checks were also done on sampled colonies from expression strain transformation. PCR screening of pET3a and pET14b genes in Rosetta strains show the expected size, indicating that the transformations into expression strains succeeded (See Figure R4).

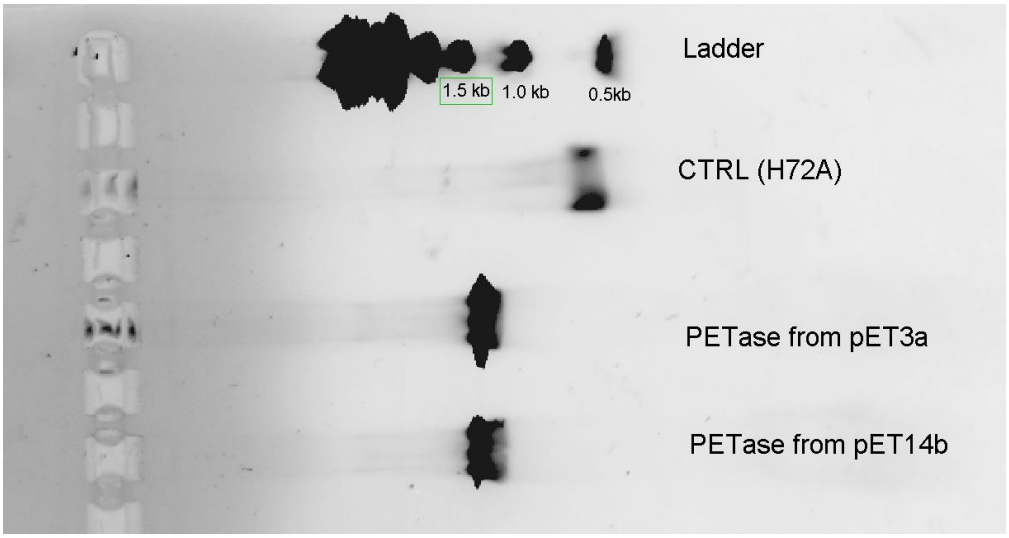

Figure R4: The pET3a and pET14b PETase genes screened from Rosetta expression strains. The result is consistent with expected based on use of T7 primers. Notice that the pET14b band is slightly larger, corroborating the extra sequence coding for the His-tag.

Sequencing

Sequencing data follows. Ligation attempts 3A and 2A of the pET3a PETase were successful with fidelity, along with a pET14 PETase and two pET28 PETase attempts. Redundant instances of successful inserts did occur but are not shown for brevity. Sequencing results of the pET3 PETase show perfect fidelity (See Figure R5). Mismatches or unknowns seen on the sequencing output were justified in context with the absorbance spectra (See supplementary data). Sequencing results of the reverse complement to the

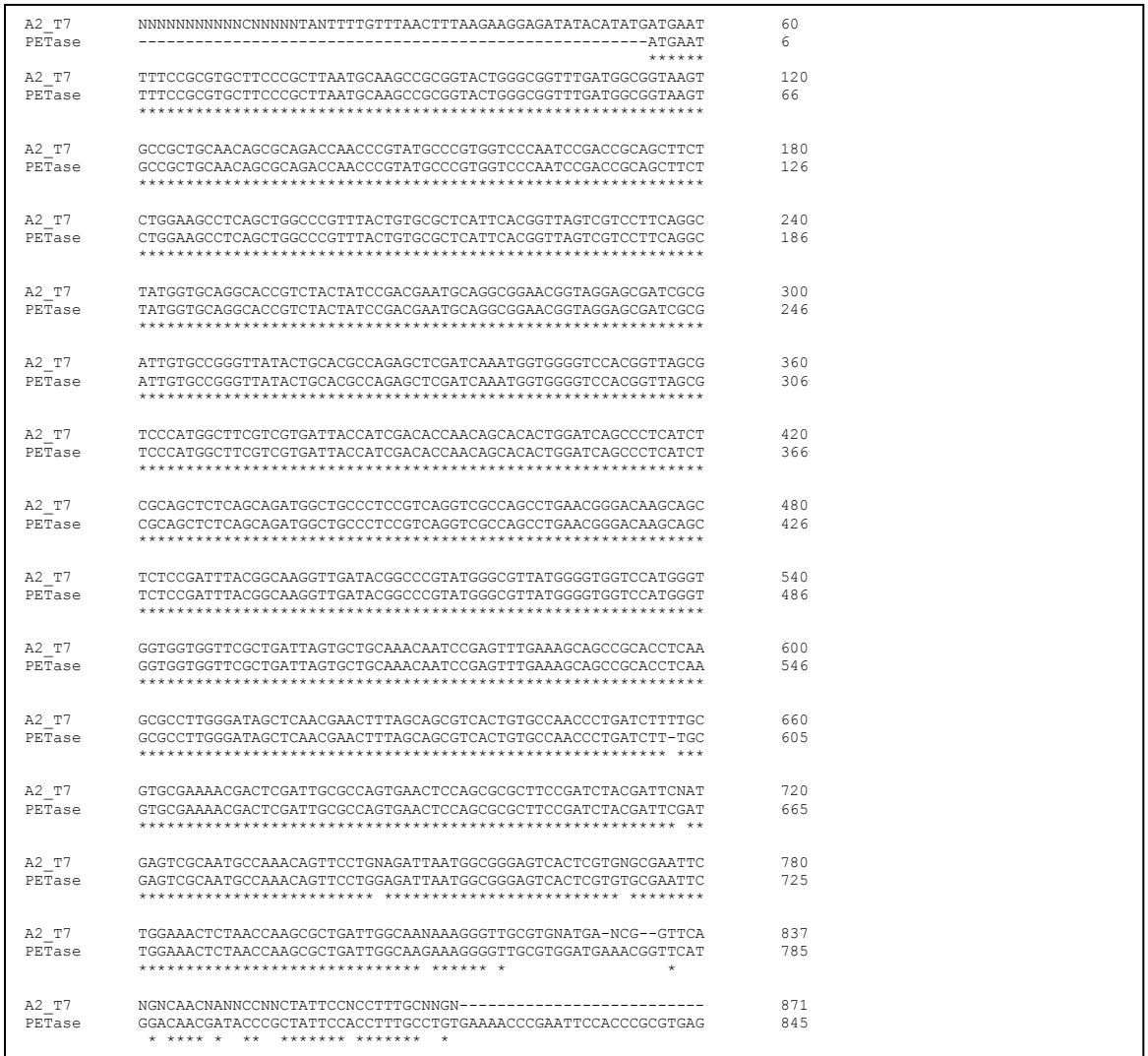

Figure R5: Sanger sequencing results of the pET3a PETase compared against predicted gene. Absorbance output can be found in Figure S3.

pET3 PETase also show perfect fidelity, accounting for mismatches or unknowns using the absorbance spectra (See Figure R6). There was no evidence of insertions or deletions anywhere in the sequence.

The pET14 PETase sequencing results showed similar fidelity (See Figure R7). Very few mismatches or unknowns were returned as outputs. Those that were found

```
A2_T7term       NNNNNNNNNNNNNNNNNNTTCNNNNTNTGTTAGCAGCCGGATCCCGAGCAATTCGCCGTGC  60
PETase          ----------------------------------------CGAGCAATTCGCCGTGC  17
                                                         *****************

A2_T7term       GAAAATCGCTCACGCGGGNGGAATTCGGGTTTTCACAGGCAAAGGTGGAATAGCGGGTAT  120
PETase          GAAAATCGCTCACGCGGGTGGAATTCGGGTTTTCACAGGCAAAGGTGGAATAGCGGGTAT  77
                ***************** ****************************************

A2_T7term       CGTTGTCCATGAACCGTTTCATCCACGCAACCCCTTTCTTGCCAATCAGCGCTTGGTTAG  180
PETase          CGTTGTCCATGAACCGTTTCATCCACGCAACCCCTTTCTTGCCAATCAGCGCTTGGTTAG  137
                ************************************************************

A2_T7term       AGTTTCCAGAATTCGCACACGAGTGACTCCCGCCATTAATCTCCAGGAACTGTTTGGCAT  240
PETase          AGTTTCCAGAATTCGCACACGAGTGACTCCCGCCATTAATCTCCAGGAACTGTTTGGCAT  197
                ************************************************************

A2_T7term       TGCGACTCATCGAATCGTAGATCGGAAGCGCGCTGGAGTTCACTGGCGCAATCGAGTCGT  300
PETase          TGCGACTCATCGAATCGTAGATCGGAAGCGCGCTGGAGTTCACTGGCGCAATCGAGTCGT  257
                ************************************************************

A2_T7term       TTTCGCACGCAAAGATCAGGGTTGGCACAGTGACGCTGCTAAAGTTCGTTGAGCTATCCC  360
PETase          TTTCGCACGCAAAGATCAGGGTTGGCACAGTGACGCTGCTAAAGTTCGTTGAGCTATCCC  317
                ************************************************************

A2_T7term       AAGGCGCTTGAGGTGCGGCTGCTTTCAAACTCGGATTGTTTGCAGCACTAATCAGCGAAC  420
PETase          AAGGCGCTTGAGGTGCGGCTGCTTTCAAACTCGGATTGTTTGCAGCACTAATCAGCGAAC  377
                ************************************************************

A2_T7term       CACCACCACCCATGGACCACCCCATAACGCCCATACGGGCCGTATCAACCTTGCCGTAAA  480
PETase          CACCACCACCCATGGACCACCCCATAACGCCCATACGGGCCGTATCAACCTTGCCGTAAA  437
                ************************************************************

A2_T7term       TCGGAGAGCTGCTTGTCCCGTTCAGGCTGGCGACCTGACGGAGGGCAGCCATCTGCTGAG  540
PETase          TCGGAGAGCTGCTTGTCCCGTTCAGGCTGGCGACCTGACGGAGGGCAGCCATCTGCTGAG  497
                ************************************************************

A2_T7term       AGCTGCGAGATGAGGGCTGATCCAGTGTGCTGTTGGTGTCGATGGTAATCACGACGAAGC  600
PETase          AGCTGCGAGATGAGGGCTGATCCAGTGTGCTGTTGGTGTCGATGGTAATCACGACGAAGC  557
                ************************************************************

A2_T7term       CATGGGACGCTAACCGTGGACCCCACCATTTGATCGAGCTCTGGCGTGCAGTATAACCCG  660
PETase          CATGGGACGCTAACCGTGGACCCCACCATTTGATCGAGCTCTGGCGTGCAGTATAACCCG  617
                ************************************************************

A2_T7term       GCACAATCGCGATCGCTCCTACCGTTCCGCCTGCATTCGTCGGATAGTAGACGGTGCCTG  720
PETase          GCACAATCGCGATCGCTCCTACCGTTCCGCCTGCATTCGTCGGATAGTAGACGGTGCCTG  677
                ************************************************************

A2_T7term       CACCATAGCCTGAAGGACGACTAACCGTGAATGAGCGCACAGTAAACGGGCCAGCTGAGG  780
PETase          CACCATAGCCTGAAGGACGACTAACCGTGAATGAGCGCACAGTAAACGGGCCAGCTGAGG  737
                ************************************************************

A2_T7term       CTTCCAGAGAAGCTGCGGTCGGATTGGGACCACGGGCATACGGGTTGGTCTGCGCTGTTG  840
PETase          CTTCCAGAGAAGCTGCGGTCGGATTGGGACCACGGGCATACGGGTTGGTCTGCGCTGTTG  797
                ************************************************************

A2_T7term       CAGCGGCACTTACCGCCATCAAACCGCCCAGTACCGCGGCTTGCATTAAGCGGGAAGCAC  900
PETase          CAGCGGCACTTACCGCCATCAAACCGCCCAGTACCGCGGCTTGCATTAAGCGGGAAGCAC  857
                ************************************************************

A2_T7term       GCGGAAANTTCATCATNNGNATATCNCCTTNTTAAAGTTAAACAAAATTATTNCTANAAG  960
PETase          GCGGAAAATTCAT-------------------------------------------------  870
                ******* *****
```

Figure R6: Reverse complement Sanger sequencing results of the pET3a PETase compared against predicted gene. Absorbance output can be found in Figure S4.

could be justified by the absorbance spectra (See supplementary data). Sequencing of the reverse complement also showed excellent fidelity (See Figure R8). Very few

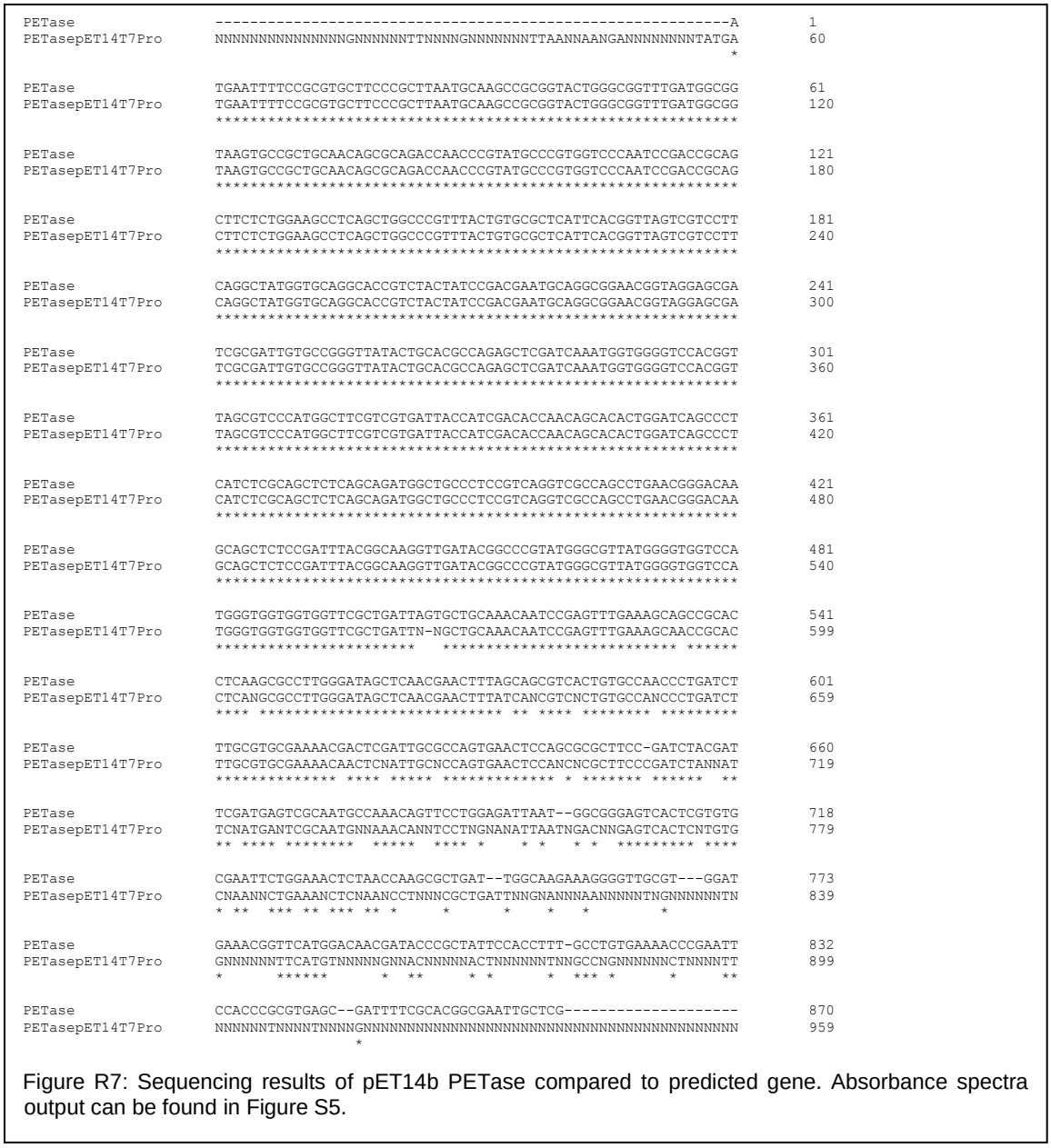

Figure R7: Sequencing results of pET14b PETase compared to predicted gene. Absorbance spectra output can be found in Figure S5.

mismatches or unknowns were seen, and again, those found were justified by absorbance spectra. No insertions or deletions were apparent.

The pET28 PETase sequencing results exhibited low signal strength, producing an incomplete map of sequence matching (See Figure R9). However, strings with sufficient signal strength showed expected homology between the constructed PETase plasmid and

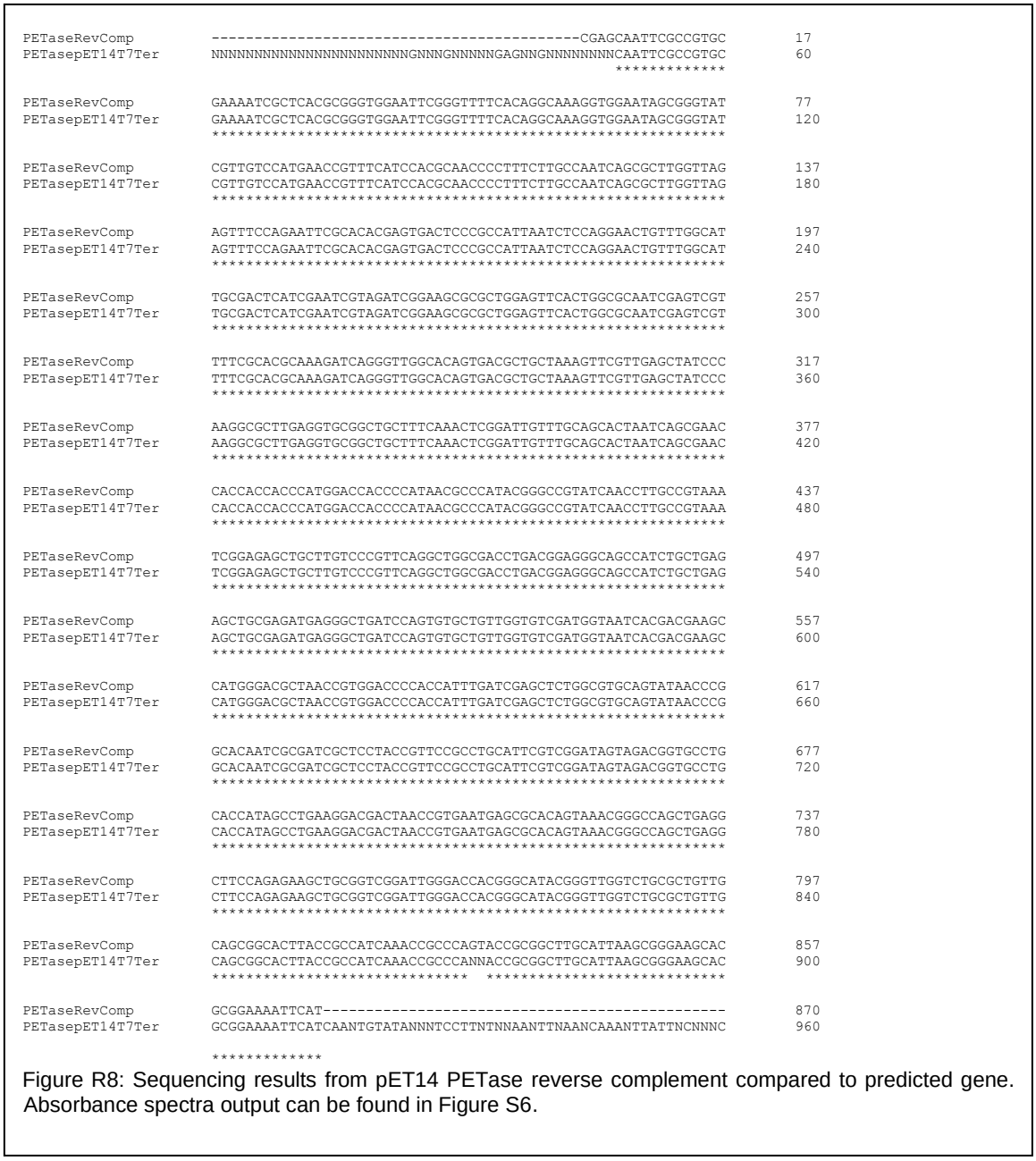

Figure R8: Sequencing results from pET14 PETase reverse complement compared to predicted gene. Absorbance spectra output can be found in Figure S6.

the PETase gene. No insertions or deletions were detected. The pET28 PETase reverse complement was also sequenced, supplementing gaps in the forward sequencing (See Figure R10). The two outputs suggest that the pET28 PETase insert occurred with fidelity, as corroborated by the absorbance spectra (See supplementary data).

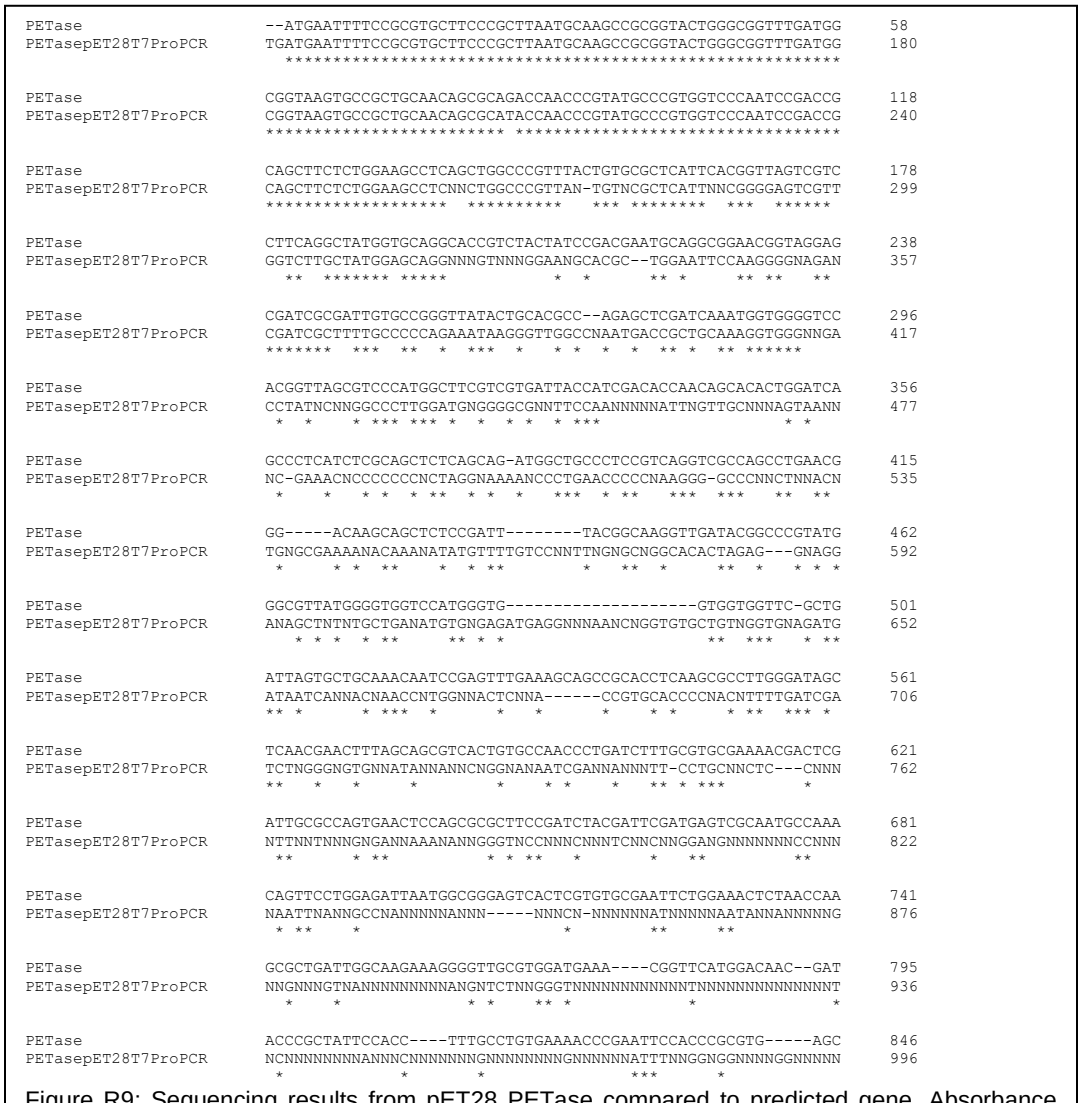

Figure R9: Sequencing results from pET28 PETase compared to predicted gene. Absorbance spectra output can be found in Figure S7.

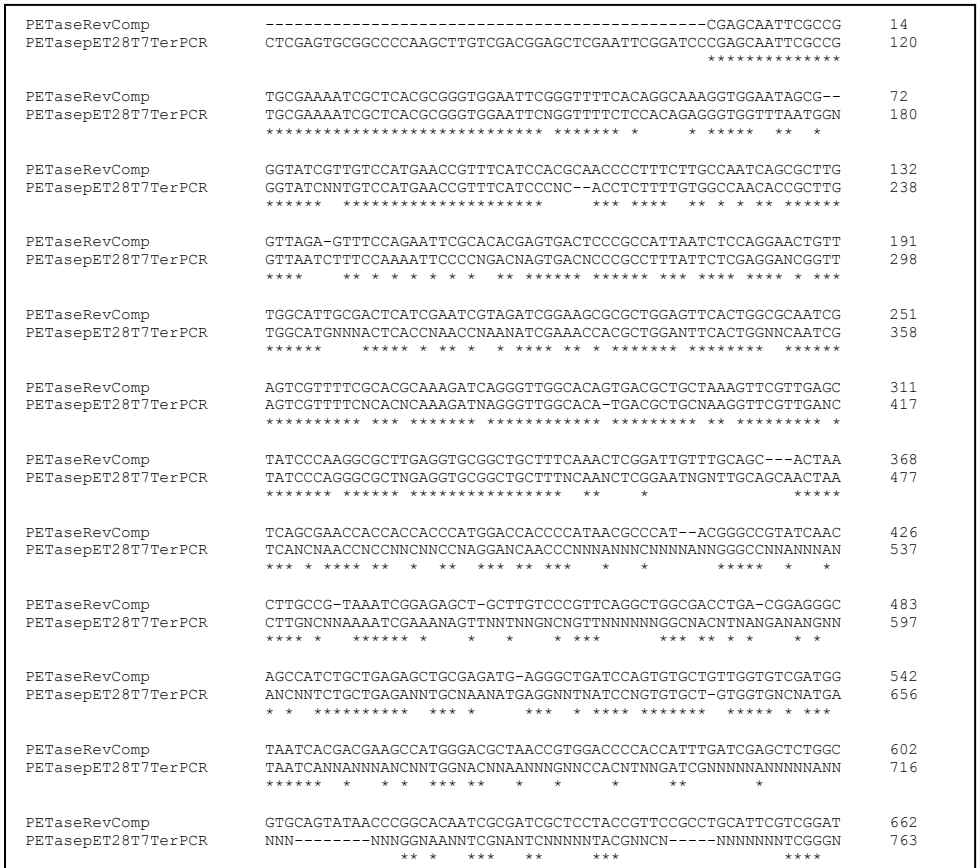

Figure R10: Sequencing results from reverse complement of pET28 PETase compared to predicted gene. Absorbance spectra output can be found in Figure S8.

Expression

Overnight induction of BL21 pET14 PETase cells was performed with 0.1mM IPTG at 16°C with shaking. After subsequent sonication, centrifuged lysate was examined by FPLC using a Ni column. Proteins eluted from Ni column during 20mM imidazole wash instead of during 300mM elution step (See Figure R11). Among the fractions measured, bands can be seen matching the expected size of PETase (~30 kDa).

Rosetta pET3 PETase cells were induced with 1.0mM IPTG at 25°C for 1-2 hours with shaking. Following sonication, centrifugation of the lysate produced an inclusion

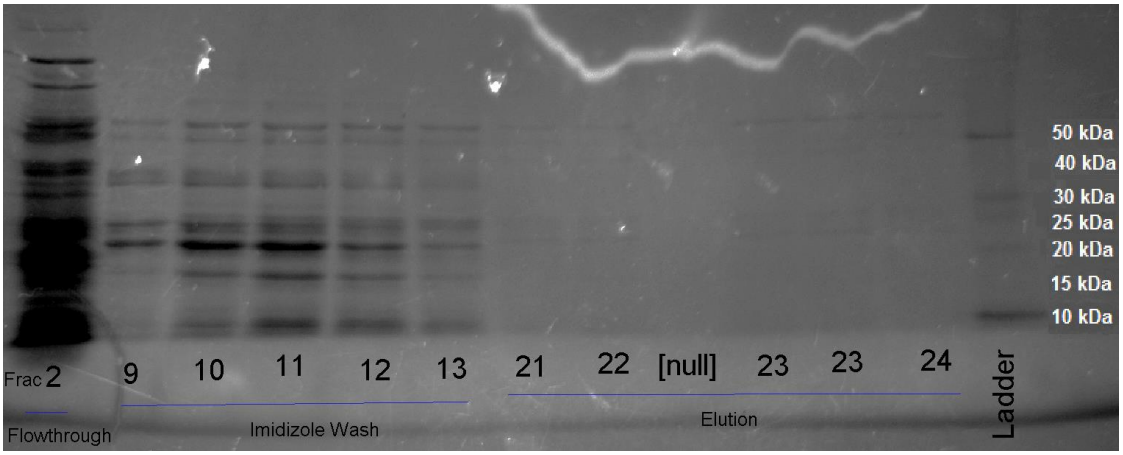

Figure R11: SDS PAGE of lysate after expression: pET14b PETase; Ni column; BL21 cells, overnight induction, 0.1mM IPTG, 16°C. Though the elution step yielded no protein, the previous flowthrough with subsequent imidazole wash eluted protein in the 25-30 kDa range consistent with the size of PETase.

body. The lysate was run by FPLC on a Q ion-exchange column. The inclusion body was run on a PAGE gel with the FPLC fractions of interest. Comparison to ladder suggests a

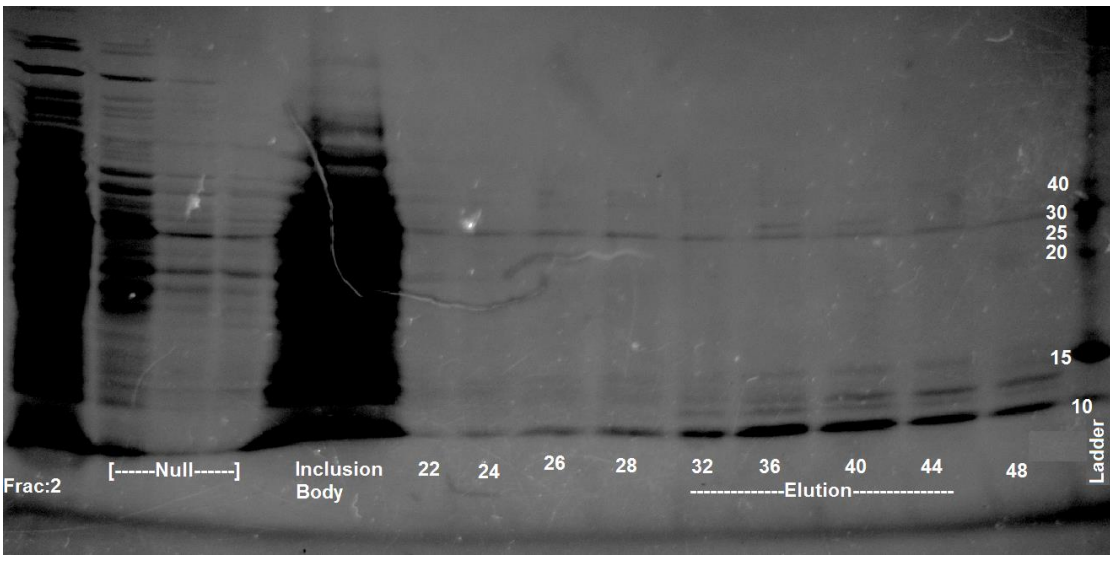

Figure R12: Lysate from Rosetta expressing pET3a PETase. This run was run on a Q ion-exchange column. The elution step shows presence of protein of expected size at fractions 36 and 40. The band running across all fractions at 30 kDa could also be the desired protein.

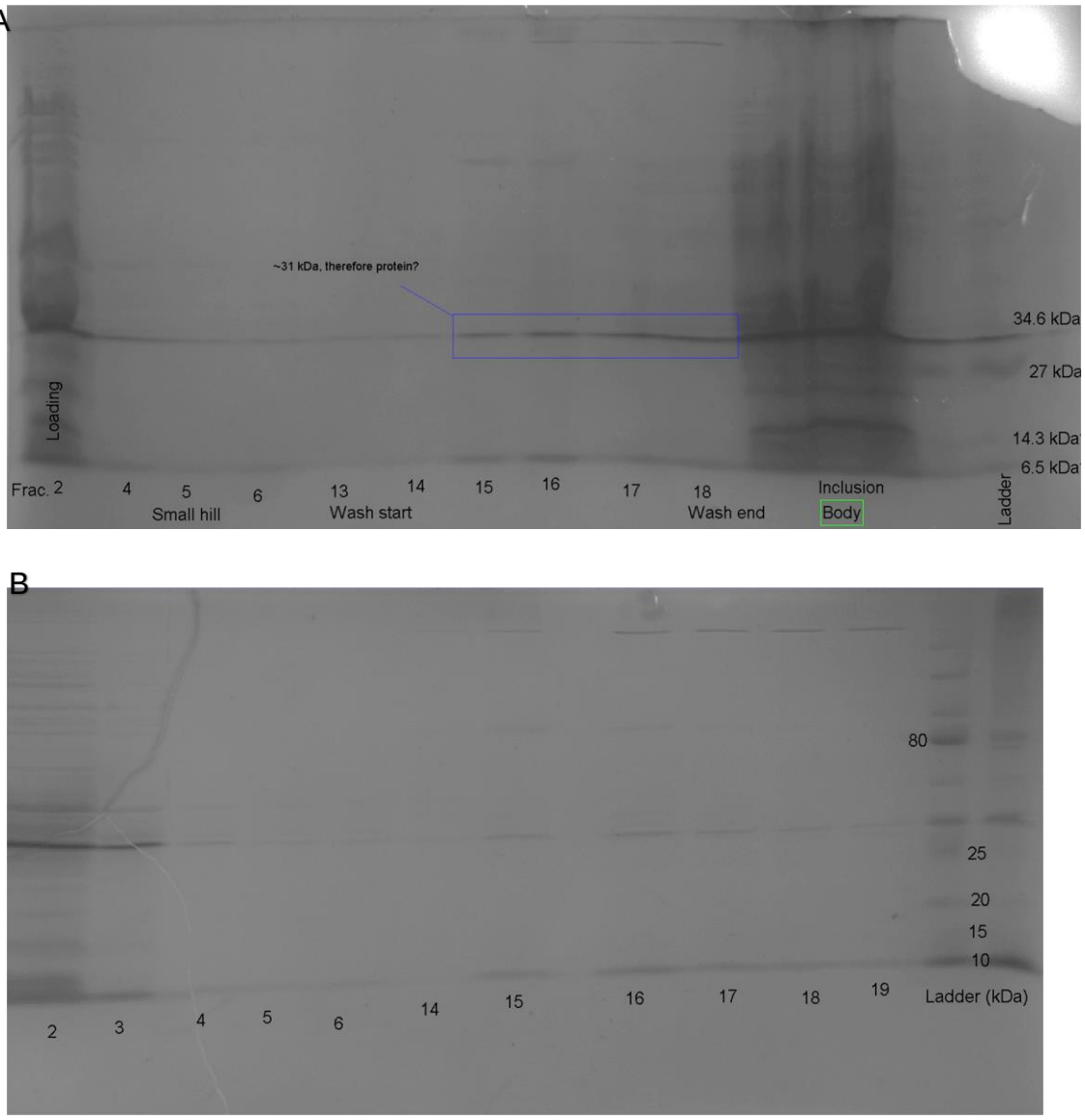

Figure R13: **A**: Lysate: NiCo cells; pET14 PETase; 0.1mM IPTG, overnight induction at 16°C with shaking; run using a Ni column. The same line across most samples can be seen at roughly 31 kDa. This line is especially prominent at the end of the wash/elution step. **B**: The lysate was run a second time, and the long prominent band persisted, suggesting that this is not an outlier. Different ladders were used to check against potential degradation of the ladder. They confirm each other.

protein of desired size at fractions 36 and 40. A thin band of ~30 kDa can also be seen across all fractions. The concentration of the inclusion body makes discerning any specific bands impossible. This is also the case for the 2nd fraction, the flow through (See Figure R12). NiCo pET14 PETase cells were induced overnight (0.1mM IPTG, 16°C with

shaking) and were lysed. Lysate was centrifuged and run on FPLC with a Ni column. Again, the inclusion body was retained and tested. For this run, the buffer was imidazole-free to allow for gradual washing. The resultant bands show the same (~30 kDa) pattern as before (See Figure R13). Despite this, confirmation by Western blot analysis failed to

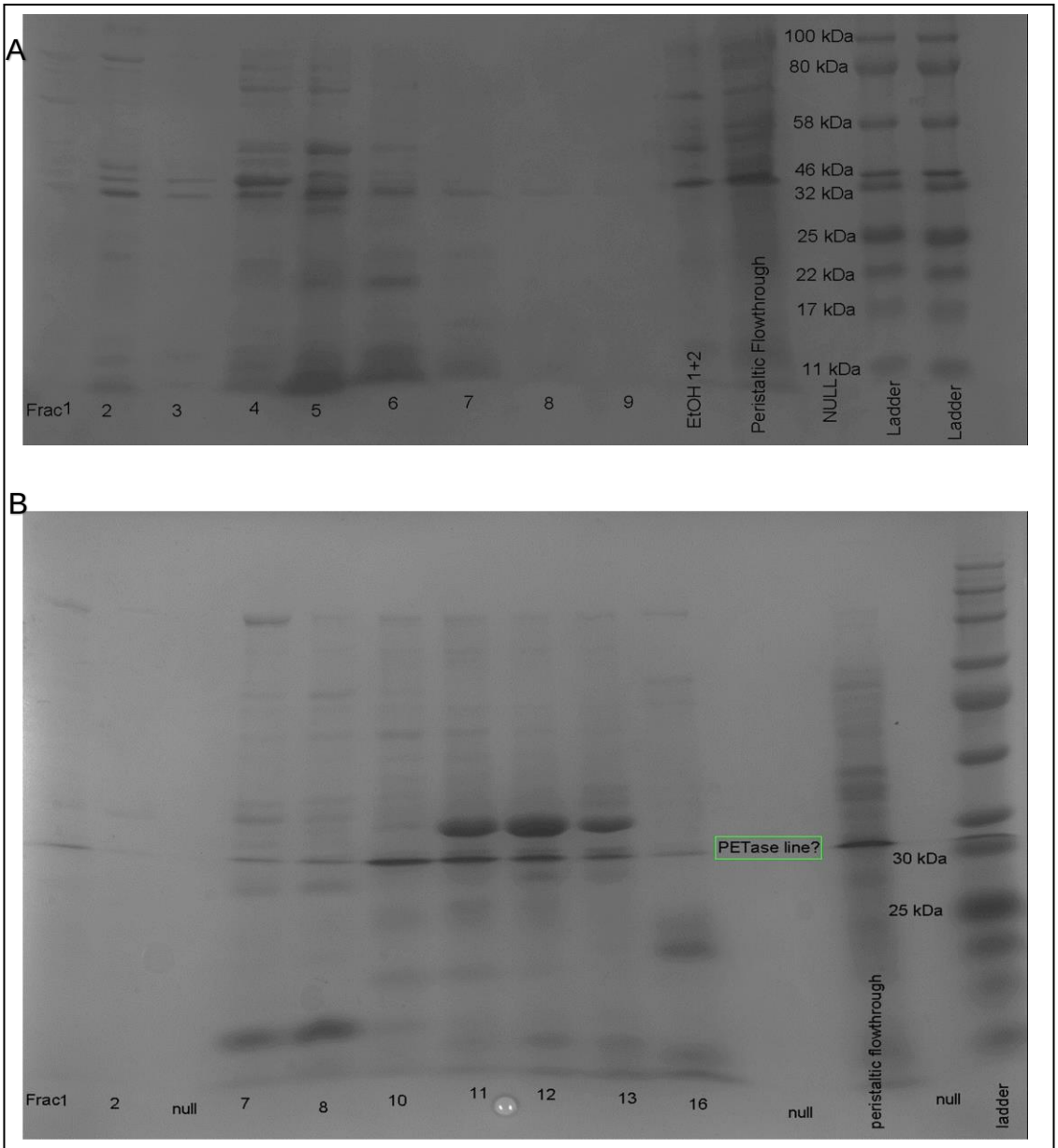

Figure R14: **A**: Lysate from NiCo expressing pET14 PETase. After washing the column with ethanol, the lysate was run through the Q ion-exchange column. The band between 30 and 40 kDa persists, suggesting that the protein of interest is present, especially in the elution fractions. **B**: A sample of the same lysate was run on an SP ion-exchange column under acidic conditions. The same series of ~30 kDa bands occurred. Fractions 11-13 also have ~36kDa bands, potentially the protein of interest.

confirm this (See Figure S12). There was, however, a dark band of low molecular weight in the flowthrough, suggesting that the protein was degraded. Potentially, the antibody concentration may have been too low to detect the protein in the fractions.

The same NiCo pET14 PETase cell stock was investigated again. The cells were cultured and induced to express overnight (0.1mM IPTG, 16°C with shaking) and were lysed. The lysate was centrifuged. The Q ion-exchange column was washed with ethanol to denature the enzyme and encourage binding. In tandem, a sample from the same lysate was run on an SP ion-exchange column. Both outputs showed the same characteristic series of ~30kDa bands, and several fractions showed a slightly larger band, 4-6 on the Q column and 11-13 on the SP column (See Figure R14).

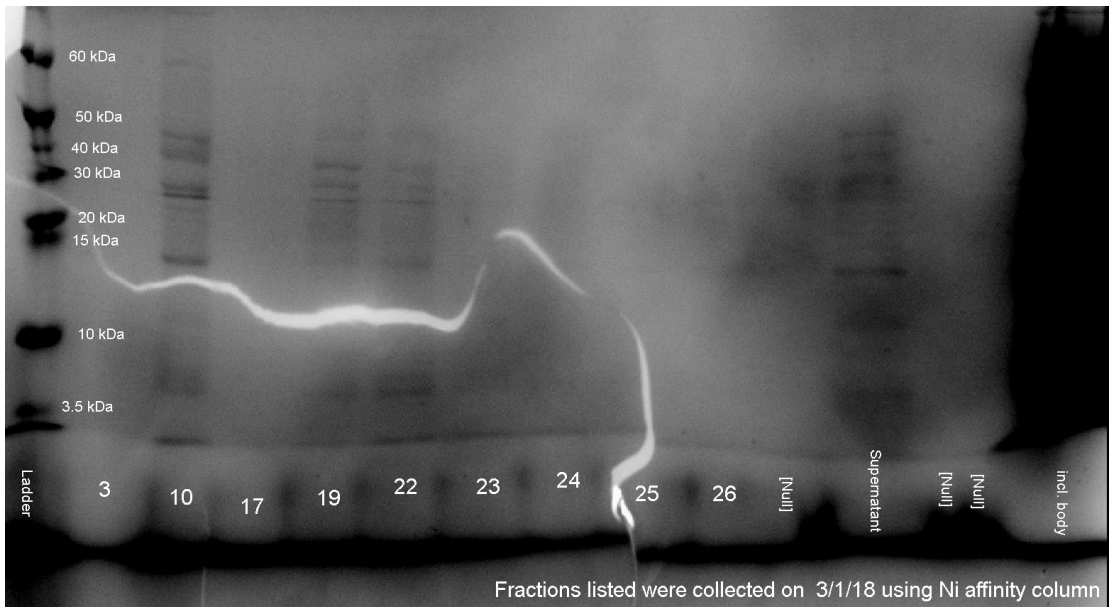

Figure R15: Lysate from BL21 expressing pET28 PETase. A faint band (~30 kDA) can be seen in the supernatant mixture, suggesting that the protein may be secreted. Fractions 10, 19, and 22 also have bands of the appropriate size.

BL21 pET28 PETase cells were induced overnight as described previously. The supernatant growth medium was also sampled and run with fractions of interest. A band of the expected size can be faintly seen in the supernatant column. The inclusion body was also run, but the result was too overexposed to resolve. Fractions 10, 19, and 22 also have bands consistent with the expected size of the protein (See Figure R15).

Predicted Protein

Phyre2 predictive protein mapping visualized with Chimera generated the following protein model, suggesting the use of a catalytic triad in a manner not unlike a

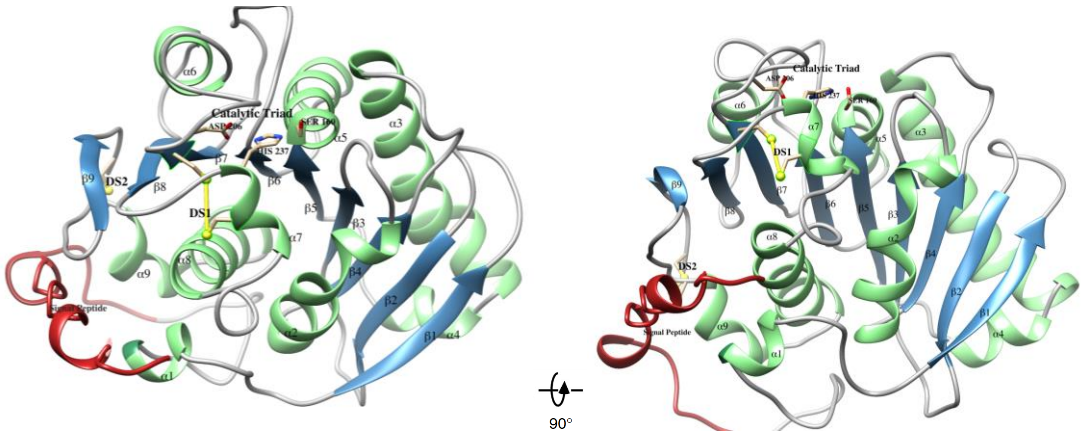

Figure R16: The expected shape of ISF6_4831 PETase. The catalytic site should be hydrophobic, allowing PET to bind. The disulfide bonds should maintain its structure when secreted, and the one close to the active site should act as structural support to exert force on the PETase. It should also help maintain precise spacing, likely necessary for the enzyme to work properly. The signal peptide can be seen at the N-terminus, in red.

textbook serine cutinase (See Figure R16). The residues facing each other in the predicted catalytic triad are S160-H237-D206. It's likely that the Ser is primed to perform a nucleophilic attack on the carbonyl carbon of the ester in PETase. The Ser is most likely primed by the His, which is most likely stabilized by the Asp. It's also reasonable to predict that the Cys facing each other will be linked as disulfide bonds; the protein will need structural support to resist degradation after secretion (Yoshida et al., 2016).

Colour Effects

After induction by IPTG, cells and media exhibited a striking pink hue. This result was replicated in every iteration of expression except in instances where transformation itself was unsuccessful. Centrifugation of cells post-induction yielded a pink pellet (See Figures

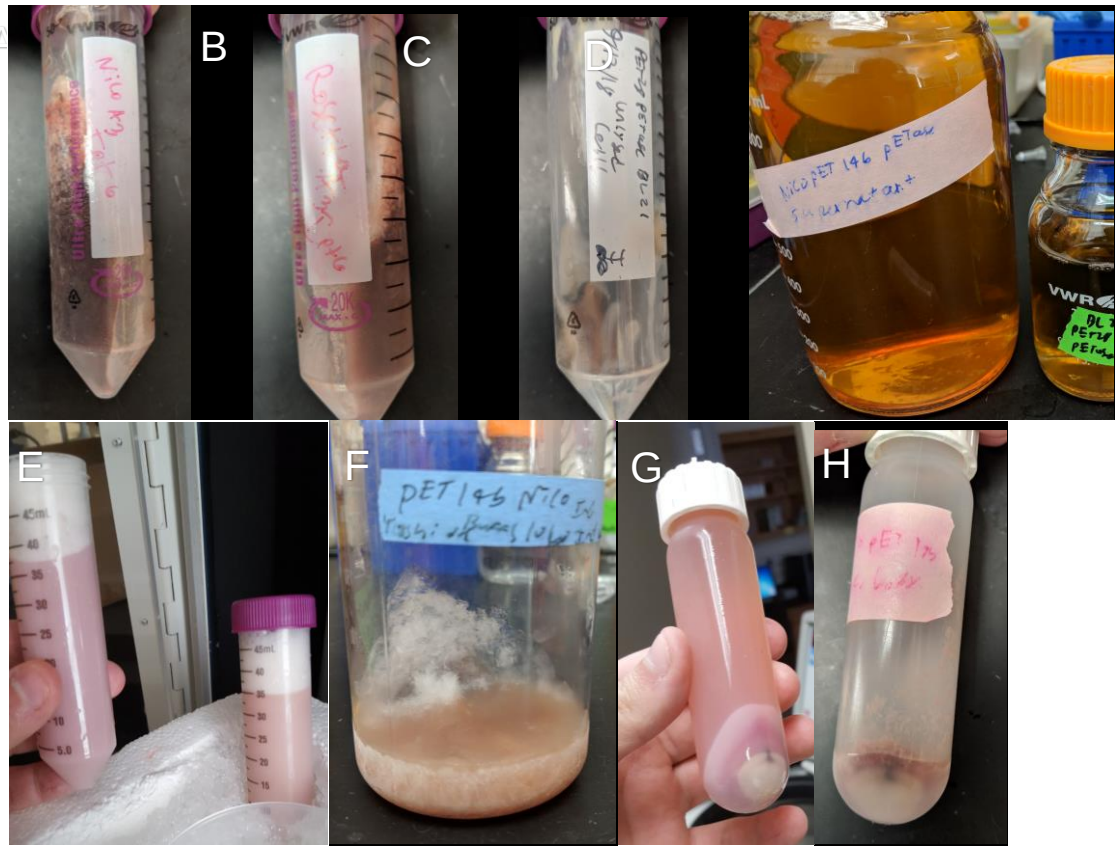

Figure R17: Examples of pink colour seen after induction. **A:** Post induction NiCo pET3 PETase cells. **B**: Post-Induction Rosetta pET3 PETase cells. **C**: Post induction BL21 pET28 PETase cells. **D**: Supernatant from NiCo pET14 PETase cells. **E**: Lysates of A and B (left and right, respectively). **F**: NiCo pET14 PETase lysate. **G**: Rosetta pET3 PETase lysate after centrifugation, showing inclusion body. **H**: NiCo pET14 PETase inclusion body.

R17A-C) with similarly pink supernatant (See Figure R17D). Lysates and inclusion bodies appeared pink as well (See Figures R17E-H). Flowthroughs of lysates from induced cells

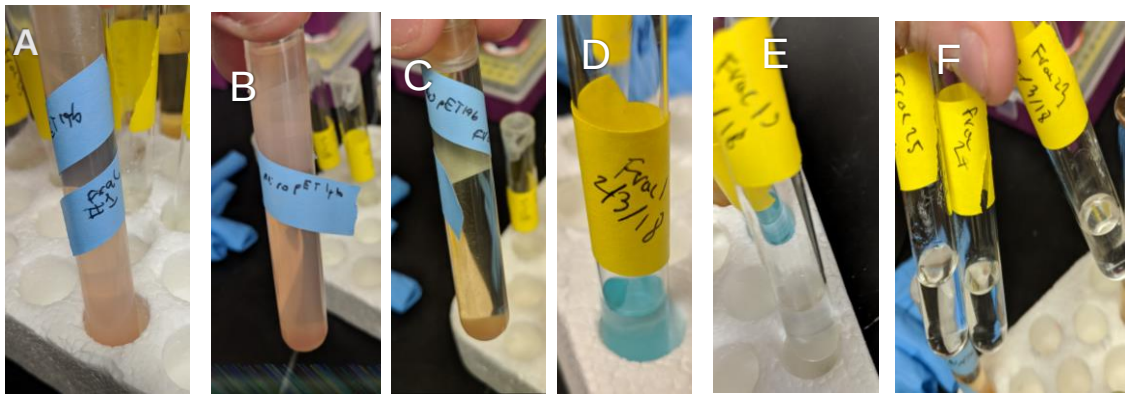

Figure R18: Fractions of interest from FPLC results. **A**: NiCo pET14 flowthrough (See Figure R13A) **B**: NiCo pET14 flowthrough. **C**: A after separation into pink layer and translucent layer. **D**: BL21 pET28 flowthrough after colour change (See Figure R15). **E**: Buffer wash runoff of BL21 pET28 lysate. **F**: Elutions of BL21 pET28 lysate.

appeared pink after filtration on FPLC (See Figure R18A+B). All non-flowthrough fractions showed no pink colour, but still appeared to contain protein of expected size (See previous gels and Supplementary Data).

The pink NiCo pET14 PETase flowthrough fractions were gathered and stored overnight at 4°C. The following morning, a turbid pink layer of liquid was visible at the bottom of the test tube (See Figure R18C). A sample was centrifuged for 30 minutes at 4700 G to isolate the pink material. Paradoxically, centrifugation resuspended the pink material. However, a white pellet was collected at the bottom of the flask. This white pellet and the pink resuspended mixture were run on a PAGE gel. Samples of isolated pink material and non-pink liquid were also extracted from an adjacent flowthrough fraction that had not been centrifuged. A sample of the post-induction growth media supernatant

was also analyzed (See Figure R19). All samples seem to contain a protein of the expected size.

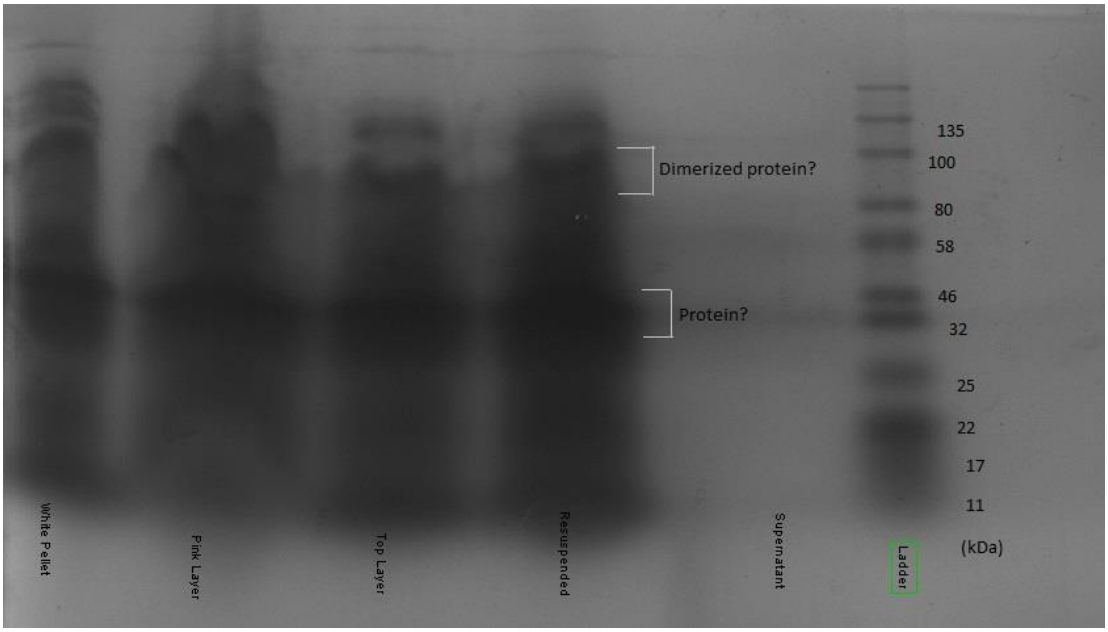

Figure R19: A series of bands can be seen at ~32 and ~90 kDa. This is potentially dimerized protein. In the supernatant, a faint band can also be seen at ~32 kDa.

In light of these results, post-induction samples of cells were methylene blue stained and examined by light microscopy. No abnormal morphologies or contaminants were apparent (See Supplementary Data).

Post-induction cells were also sampled and cultured in non-LB media. These exhibited a mossy green hue after incubation at room temperature overnight without shaking (See Supplementary Data). In a separate experiment, post-induction cells were further incubated at 4°C for two days without changing growth media, without shaking. The cold cell culture tubes exhibited a cyan colour (Figure not shown).

Figure R20: NiCo pET14 cells show green on overgrown areas of plate.

Cells were plated on antibiotic-free media and grown at 37°C overnight, while monitoring for colour changes. A subtle green hue was seen in overgrown areas of the plate (See Figure R20).

In an attempt to replicate the cyan results ex vivo, elutions and flowthroughs from pET28 PETase BL21 cells were held at 4°C for two days without shaking. Flowthrough fractions exhibited the same characteristic cyan colour seen in cold, post-induction, living cell cultures (See Figure R18D).

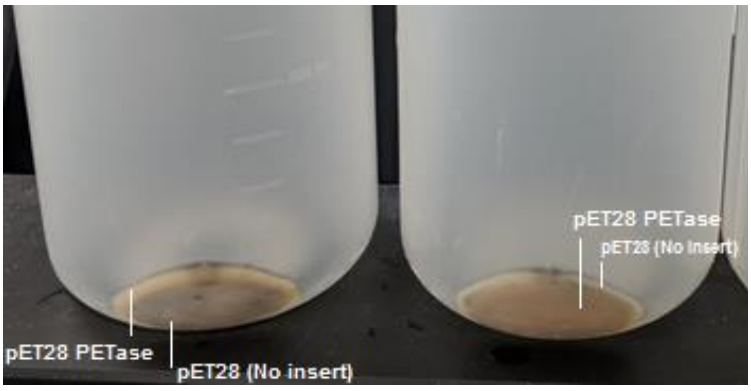

Figure R21: The pET28 BL21 cell conditions after induction and centrifugation. The pink colour can be seen in the PETase$^{(+)}$ cells. The PETase$^{(-)}$ cells appear grey.

BL21 pET28 PETase cells were grown, induced, and pelleted. BL21 pET28 cells containing no insert received the same treatment. In a second centrifugation step, the PETase BL21 media was added to the negative control and vice-versa. This allowed for easier side-by side comparison (See Figure R21).

Cells were also grown with a signal-free version of the PETase. PET15 and pET28 signal-free PETase vectors were cloned into BL21 expression strains and induced overnight at 16°C. After cell harvesting and lysis, the resultant lysate appeared pink. Pre-lysis, the cell suspension appeared grey (See Figure R22).

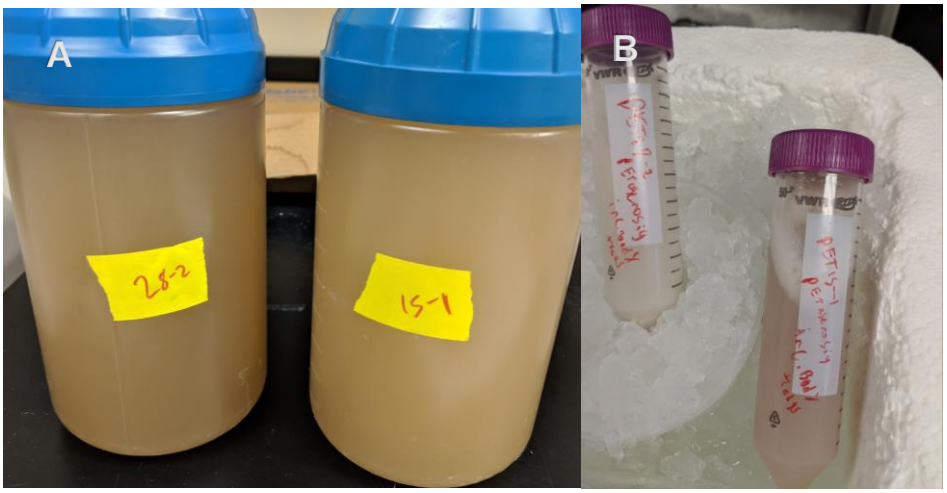

Figure R22: BL21 cultures of PETases with no signal induced overnight at 16°C. 16 **A:** Left: pET28 PETase culture after induction. Right: pET15 PETase culture after induction. **B:** Left: pET28 PETase, unlysed. Right: pET15 PETase, lysed. The pink colour can be clearly seen in the lysed sample, but not the unlysed one.

Discussion

ISF6_4831 was successfully ligated into three different plasmids for varying types of expression and purification. These plasmids, pET3, pET14, and pET28, have been sequenced and shown to contain the correct insert. Although sequencing data for the pET14 and pET28 plasmids wasn't perfect, sequencing in both directions and examining the spectra in detail suggested that the insert is correct. Results suggest transformations into expression and storage strains of *E. coli* were successful. This fulfills one of the goals of the project because it provides a reliable method for subsequent exploration of the gene and its associated protein. Stocks of plasmids have been made and stored for future transformations. Future Winthrop students will be able to express and purify the protein and study it in a research setting should they choose to do so.

It has been claimed that ISF6_4831 acts on very few substrates non-PET substrates. Nonetheless, it was our intention to use PNPP as a pathway to assay for effectively confirming enzyme activity (Yoshida et al., 2016). In addition to the direct spectrophotometric analysis, we planned to use high performance liquid chromatography (HPLC) analysis for a parallel assay to provide interspersed snapshots of the activity of PETase on its natural substrate (Bagheban-Shahri, Niazi, and Akrami; 2012). The combination of these two assays was to provide a quantitative and qualitative understanding of the enzyme activity and will allow us to draw conclusions regarding the potential of this biochemical system to be used on the commercial scale for the biodegradation of PET plastics (Cornish-Bowden, 2014). Although this goal was not fully realized due to purification issues, two competing papers published during the last two

months of the project timeline demonstrated that this was experimentally possible (Joo, 2018; Han, 2017).

Both papers focused on the PETase mechanism of action, utilizing x-ray crystallography, molecular modeling, and site-directed mutagenesis. One paper even directed a mutagenesis to the active site that decluttered landing and increased activity (Joo, 2018), suggesting that this enzyme's efficiency can still be improved by intuitive modification. Our proposed mechanism of action and structure as generated by Phyre2, Chimera, and deduction was corroborated by these two articles. This enzyme relies on a catalytic triad to cleave PET at the carbonyl carbon, the ester bond. This is facilitated by a tryptophan "spatula" that moves substrate in and product out by use of T-stacking and face-to-face stacking. This Trp is unique to PETase (Han, 2017). Large dimers on SDS PAGE results coupled with pairs of closely-coordinated Cys residues led us to predict a protein stabilized by two disulfide bonds. It has been postulated that their role isn't purely architectural, and that they help organize precise spacing near the active site, partially explaining PETase's high rate of activity compared to other similar enzymes. Furthermore, the prediction of a large hydrophobic cleft capable of holding several plastic monomers was correct (Joo, et al., 2018).

Perhaps the most surprising result was the fact that induction was always closely followed by the appearance of a pink colour. Occurring without fail about an hour after room-temperature induction and the next morning with cold inductions, these pink results have never been documented before. Admittedly, research on this is sparse. It's possible that the pink effect was seen by Yoshida et al. (2016), who were more interested in purifying the protein to contextually describe *I. sakaiensis*, rather than coming up with their

own systematic platform for non-native PETase expression and purification. The authors of the other two papers, however, were examining the enzyme directly, with only cursory discussion of its origin. If they had seen this colour, they would have almost certainly mentioned it. Considering the brevity with which all three papers discussed their methods, it's possible this result could have been discounted in the Yoshida paper, but not the others. Since there is no mention, even in passing, of this pink colour, I don't believe that any of them saw it at all (Han, 2017; Joo, 2018).

Yet, this striking pink colour persistently appeared in every successful induction of PETase protein. There was no evidence of contamination; the cultures were inoculated in sterile conditions and screened with antibiotics. Also, pET28 confers resistance to a different antibiotic, kanamycin, and the pink colour was seen with induction from those cells as well. It's unlikely that there's a common prokaryotic contaminant that is resistant to both antibiotics and produces a pink colour. Eukaryotic contaminants are also not present. The cell pellets after centrifugation are one contiguous mass. Had the culture been heterogeneous, the pellet would have displayed obvious layers. *Bacillus thuringiensis* can sometimes appear pink after lysis (Iriarte, 2000), so the cells were also stained using methylene blue, and light microscopy (100x) showed no morphological abnormalities or apparent contaminants. It's unlikely that a defect in the sequence is responsible. The gene has been ligated into three separate plasmids, with PCR and sequencing data (in both directions) confirming the correct insertion. For each of these conditions, the pink colour was seen. It's unlikely to be a defect in the cell stocks either because naïve cells did not display the pink colour, and all three expression strains (BL21, Rosetta, and NiCo)

produced the pink effect. Therefore, qualms about the legitimacy of the pink colour can be assuaged.

Fractions that showed pink (flowthroughs) were often found to contain a protein of the expected size, except in cases where they were simply unreadable due to overexposure. We explored the possibility that the protein itself may be pink. This can occur when metal ion cofactors are present. Bizarrely, *E. coli* has the potential to use manganese, vanadium, or even uranium ions as cofactors in proteins (Cvetkovic, 2010). However, its unlikely PETase is an example of this phenomenon. Although a pink colour appears when the protein does, subsequent clear elution fractions seemed to contain a band of the correct size. However, even if the supposed bands of interest from non-pink fractions are false positives, it's unlikely the protein is pink because it has been crystallized and has not been demonstrated to use any cofactors (Han, 2017). Our molecular modeling work corroborates this. Furthermore, homologous PETases do not use cofactors (Joo, 2018).

The most likely reason for the pink effect is informed by the other colours witnessed: green and cyan. These odd results suggest that the expressed PETase demonstrated nonspecific activity on a native "bystander" molecule, perhaps in the growth media, and hydrolyzed it, producing a chromophore. This hypothetical chromophore precursor likely had a benzene ring with an ester group attached to it, not unlike PET. PNPP fits these criteria, and PETase has documented marginal activity on it, demonstrating its ability to generate chromophores for activity assays (Han, 2017). When the induced cells were cultured in different media, it's likely that a green colour was observed because different chromophore precursors were present. When the cells were incubated at 4°C,

conformational changes may have taken place in the enzyme, altering its affinity and hydrolyzing a different chromophore, producing cyan.

The signal peptide most parsimoniously explains why our lab witnessed a pink effect that the previous authors did not document. Because *I. sakaiensis* and *E. coli* are both gram-negative bacteria, signal sequences are said to be somewhat conserved between them (Juncker, 2003). This has been convenient for previous research on this protein, because it allowed the signal portion of the gene to be reliably predicted and cleaved before investigation (Han, 2017). However, previous one-dimensional approaches to expressing and purifying the protein – either to answer phylogenetic questions or mechanistic ones – have relied entirely on predictive algorithms for experimental design. This meant that no paper had experimentally confirmed the predictions made by signal-finding algorithms. Put simply: it was uncertain whether *E. coli* could express and secrete an active PETase because no one bothered to check. Somewhat inadvertently, we have accomplished that. This potentially explains why no research group has discussed this pink effect thus far. It's possible that the pink shift is only be seen when the protein interacts with LB media, where it can hydrolyze molecules in the cocktail of peptides, peptones, and vitamins that feed the culture. This is corroborated by the final finding, suggesting that in the absence of the signal, the enzyme is contained almost exclusively in the cells, and that upon lysis, the released enzymes react with trace amounts of the media to produce the observed pink colour.

Future Directions

In the short term, future directions could focus on proper purification and characterization as was the original goal for this study. This includes running an osmotic shock test to determine whether the non-signaled protein is housed in the periplasmic space or in the cytoplasm following expression (Ewis, 2005). Following through with this objective may provide pathways for other stated goals to be achieved, including the confirmation of PNPP as a potential laboratory assay for activity and the measurement of PETase on its native substrate (Bowers, 1980). Furthermore, these studies will necessarily produce a supply of MHET, allowing for substrate to test an MHETase, the second step in this enzyme pathway. Without an active form of PETase, MHETase studies – of which there are none – cannot be performed. These projects could be supplemented with immunohistochemistry methods, such as Western blotting and ELISAs.

If correct, the fact that *E. coli* can express and secrete an active form of this enzyme provides a potential platform for industrial recycling. Instead of the current approach to PET plastic recycling, – where materials are collected, sorted, cleaned, and remelted and/or repolymerized – recycling plants could simply grind up their waste (even if it was mixed-media) and pour it into an active culture bath. The PET would be hydrolyzed into MHET, rendering it water-soluble (US EPA, 2018). The culture would then be centrifuged. All the cells and non-PET would collect at the bottom, and the MHET-containing media could be decanted and purified. Potentially, this saves a massive amount of waste since it skips the sorting step, even allowing PET from heterogeneous products to be recovered. A similar approach could potentially be effective for intervention in polluted waterways, oceans, beaches, and other environments cluttered up with PET waste. This is a more difficult

problem, because it essentially turns an insoluble pollutant into a soluble one. That having been said, more research needs to be done to determine whether the risks of a potential influx of MHET would outweigh the benefits of removing all the PET in a polluted aquatic environment.

However, all of this implies that the gene could be transferred into *E. coli* without any apparent change in the sequence. Indeed, it might not directly require human intervention at all. Experiments in bioremediation of toluene have shown toluene-degrading genes propagate across similar species – via horizontal gene transfer – when an abundance of toluene is present (Taghavi, 2005). The same effect could conceivably occur here. Already, almost 70 PETase-like enzymes have been postulated by phylogenetic analysis (Joo, 2018), but the potential for direct interspecies transfer suggests far more. PET is one of the most abundant potential untapped food sources in the world. It's possible that *I. sakaiensis* isn't the only plastic-eating creature in that landfill. Phylogenetics PETase research suggests that it is not (Danso, 2018).

Efforts to generate a PETase gene without the signal sequence have shown preliminary success, so purification of the resultant protein should be much easier than from a signaled PETase. If that is the case, it would further corroborate the claims made here. Other considerations include the second step of the PET-degradation pathway, MHETase. Research into MHETase is still in its infancy, even compared to PETase. This is partially the case because PET degradation is currently the only way to isolate samples of MHET for testing MHETase (Yoshida, et al., 2016). It's also possible that MHETase itself may not be needed for full PET recycling. Many of the properties of MHET haven't been experimentally determined, so the potential for its use as an ingredient in recycling

outside of enzymatic degradation is wholly unknown. Coupled with MHETase, this would be an excellent direction for future research.

Regardless of ISF6_4831's specific future as a tool for bioremediation, discovery and investigation of this gene and its associated protein cast a fascinating light on the large-scale fundamentals of ecology and the carbon cycle. PET bottles were invented in the past 50 years (Forrest, 2016), and the recycling plant surveyed was built less than 30 years ago (Tanaka, 1999). The analyzed sites were contaminated with plastic only five years prior to the screening experiment (Yoshida, et al., 2016). Despite this, organism(s) have already appeared that can degrade the plastic wastes there. This is an optimistic development in the conflict that is industrialization vis-à-vis the environment. Potentially, for many of the environmental problems we've created, a solution is already evolving. We simply must find it (Danso, 2018).

Statement of Intellectual Property Rights

The author of this thesis reserves all rights to intellectual property, physical or intangible, generated by this project. This includes (but is not limited to) genetic sequences, organisms, proteins, reagents, metabolites, byproducts, protocols, and processes. Any and all potential inventions or innovations based on – or resulting from – data generated by this research, either directly or indirectly, are property of the original thesis author: Nathan Koconis.

Works Cited

Agilent Technologies. Agilent Cary 60 Spectrophotometer user's guide. Retrieved from http://www.agilent.com/cs/library/usermanuals/public/G6860-90001.pdf.

Augé, A.A (2017). Anthropogenic debris in the diet of turkey vultures (*Cathartes aura*) in a remote and low-populated South Atlantic island. *Polar Biology, 40*(4), 799-805. Retrieved from https://doi-org.winthropuniversity.idm.oclc.org/10.1007/s00300-016-2004-0

Bagheban-Shahri, F., Niazi, A., Akrami A (2012). Simultaneous spectrophotometric determination of nitrophenol isomers in environmental samples using first derivative of the density ration spectra. *Journal of Chemical Health Risks, 2*(4), 21–28. Retrieved from http://www.jchr.org/index.php/JCHR/article/view/95.

Barreiros, J. P., & Luiz, O. J. (2009). Use of plastic debris as shelter by an unidentified species of hermit crab from the Maldives. *Marine Biodiversity Records, 2*(1). doi:10.1017/S1755267208000377

Bio-Rad. A guide to polyacrylamide gel electrophoresis and detection. Retrieved from http://www.biorad.com/webroot/web/pdf/lsr/literature/Bulletin_6040.pdf.

Bowers, G., McComb, R., Christensen, R., Schaffer, R. (1980). High-purity 4-nitrophenol: purification, characterization, and specifications for use as a spectrophotometric reference material. *Clinical Chemistry, 26*(6), 724–729. Retrieved from https://www.ncbi.nlm.nih.gov/pubmed/7371150

Chae, Y., & An, Y. J. (2017). Effects of micro-and nanoplastics on aquatic ecosystems: Current research trends and perspectives. *Marine Pollution Bulletin, 124*(2), 624-632.

Chan, W. T., Verma, C. S., Lane, D. P., & Gan, S. K. E. (2013). A comparison and optimization of methods and factors affecting the transformation of Escherichia coli. *Bioscience Reports, 33*(6), e00086. http://doi.org/10.1042/BSR20130098

Chen R. (2011). Bacterial expression systems for recombinant protein production: E. coli and beyond. *Biotechnology Advances, 30*(5), 1102–1107.

Cornish-Bowden, A. (2014). Analysis and interpretation of enzyme kinetic data. *Perspectives in Science, 1*(1-6), 121–125.

Davis, M. (2013). A plasmid editor. *Biology Labs, University of Utah.* Retrieved from: http://biologylabs.utah.edu/jorgensen/wayned/ape/

Ewis, Hosam E., Chung-Dar, L. (2005). Osmotic shock: A mechanosensitive channel blocker can prevent release of cytoplasmic by not periplasmic proteins. *FEMS Microbiology Letters, 253*(2), 295-301. doi:10.1016/j.femsle.2005.09.046

Eurofins Scientific (2017). Eurofins genomics. Retrieved from www.eurofinsgenomics.com/en/home/?ForceRecommendation=False

Forrest, M. (2016). *Recycling of polyethylene terephthalate*. Shawbury, Shrewsbury, Shropshire, U.K.: Smithers Rapra.

GE Healthcare Life Sciences (2018). HiTrap IMAC sepharose FF. *GE Healthcare Life Sciences.* Retrieved from www.gelifesciences.com/en/us/shop/chromatography/prepacked-columns/affinity-specific-groups/hitrap-imac-sepharose-ff-p-03636?current=17092104

GeneTex (2013). 6X his tag antibody [3H2201]. *Antibody Supplier - GeneTex Inc.* Retrieved from www.genetex.com/6X-His-tag-antibody-3H2201-GTX15149.html

Gold, A. (1967). *Methods in enzymology* (vol. 11), 706.

Grossoehme N. (2016). Protein purification: Cell lysis through chromatography.

Han, X., Liu, W., Huang, J., Ma, J., Zheng, Y., Ko, T., & Guo, R. (2017). Structural insight into catalytic mechanism of PET hydrolase. *Nature Communications*, *8*(1), 2106. doi:10.1038/s41467-017-02255-z

Hwang, E.I., Kaneko, M., Ohnishi Y., Horinouchi, S. (2003). Production of plant-specific flavanones by *Escherichia coli* containing an artificial gene cluster. *Applied and Environmental Microbiology*, 69(5), 2699–2706.

IBI Scientific (2018). Hi-speed mini plasmid kit – 300 preps. Retrieved from www.ibisci.com/products/hi-speed-mini-plasmid-kit-300-preps

Jennings, S., Melin, F., Blanchard, J.L., Forster, R.M., Dulvy, N.K., Wilson, R.W. (2008). Global-scale predictions of community and ecosystem properties from simple ecological theory. *Proceedings of the Royal Society B: Biological Sciences*, *275*(1641), 1375–1383.

Joo, S., Cho, I. J., Seo, H., Son, H. F., Sagong, H., Shin, T. J., & Kim, K. (2018). Structural insight into molecular mechanism of poly(ethylene terephthalate) degradation. *Nature Communications*, *9*(1), 382. doi:10.1038/s41467-018-02881-1

Juncker, A. S., Willenbrock, H., Von Heijne, G., Brunak, S., Nielsen, H., & Krogh, A. (2003). Prediction of lipoprotein signal peptides in Gram-negative bacteria. *Protein Science*, *12*(8), 1652-1662.

MacArthur, E., Wraughray, D., Stuchtey, M.R. (2016). The new plastics economy: Rethinking the future of plastics. *Industry Agenda of the World Economic Forum*.

New England BioLabs. BL21 (DE3) competent *E. coli* data sheet. Retrieved from https://www.neb.com/~/media/Catalog/AllProducts/0B28021B9A36470BB46B318DAD19ED4F/Datacards%20or%20Manuals/C2527Datasheet-Lot21.pdf

New England BioLabs. NiCo21 (DE3) competent *E. coli* data sheet. Retrieved from https://www.neb.com/~/media/Catalog/All-Products/DC9A4E9F1FEE45538671E6E576ADFA14/Datacards%20or %20Manuals/C2529Datasheet-Lot5.pdf

New England BioLabs. High efficiency transformation protocol (C2529) data sheet. Retrieved from https://www.neb.com/protocols/2012/05/31/high-efficiency-transformation-protocolc2529

New England BioLabs. Optimizing restriction endonuclease reactions. Retrieved from https://www.neb.com/protocols/2012/12/07/optimizing-restriction-endonucleasereactions

New England BioLabs. Quick ligation protocol (M2200) data sheet. Retrieved from https://www.neb.com/protocols/1/01/01/quick-ligationprotocol

New England Biolabs. Unstained protein ladder, broad range (10-250 KDa). Retrieved from www.neb.com/products/p7703-unstained-protein-ladder-broad-range-10-250-kda#Product%20Information.

New England BioLabs. 5-alpha competant *E. coli* (subcloning efficiency). Retrieved from www.neb.com/products/c2988-neb-5-alpha-competent-e-coli-subcloning-efficiency#Product%20Information

Novagen. Competent cells. Retrieved from https://www.med.unc.edu/pharm/sondeklab/files/resourcefiles/manuels/novagen_competent_cells2

Novagen. pET system manual (11th ed.) Retrieved from https://www.researchgate.net/file.PostFileLoader.html?id=57583e23cbd5c22d1e72d84f&assetKey=AS%3A370732262543362%401465400867623

Novagen. pET-14b vector. Retrieved from http://www.helmholtz-muenchen.de/fileadmin/PEPF/pET_vectors/pET-14b_map.pdf

Papaneophytou, C.P., Kontopidis, G. (2013). Statistical approaches to maximize recombinant protein expression in *Escherichia coli*: A general review. *Protein Expression and Purification, 94*, 22–32.

Pettersen, E.F., Goddard, T.D., Huang, C.C., Couch, G.S., Greenblatt, D.M., Meng, E.C., and Ferrin, T.E. (2004). UCSF chimera – A visualization system for exploratory research and analysis. *Journal of Computational Chemistry, 25*(13), 1605-1612.

Phyre2 web portal for protein modeling, The, prediction and analysis Kelley LA et al. Nature Protocols 10, 845-858 (2015)

Prata, J. C. (2018). Airborne microplastics: Consequences to human health. *Environmental Pollution, 234*, 115-126.

Sigler, M. (2014). The effects of plastic pollution on aquatic wildlife: Current situations and future solutions. *Water, Air, and Soil Pollution, 225*, 2184. https://doi-org.winthropuniversity.idm.oclc.org/10.1007/s11270-014-2184-6

Sigma-Aldrich (2018). Sample preparation in ion exchange chromatography. *GE Healthcare*. Retrieved from www.sigmaaldrich.com/technical-documents/protocols/biology/ion-exchange-chromatography/appendix1.html.

Record of polyethylenterephthalate. GESTIS Substance Database of the Institute for Occupational Safety and Health, accessed on 7 November 2007

USB Corporation. PrepEase histidine-tagged protein purification kits - High specificity. Retrieved from https://www.neb.com/~/media/Catalog/All-Products/DC9A4E9F1FEE45538671E6E576ADFA14/Datacards%20or%20Manuals/C2529Datasheet-Lot5.pdf.

US EPA (2018). Estimation programs interface suite for Microsoft Windows, v 4.11. *United States Environmental Protection Agency*.

Welle, F. (2011). Twenty years of PET bottle to bottle recycling—An overview. *Resources, Conservation, and Recycling, 55*(11), 865–875.

Whitehead, T. O., Biccard, A., & Griffiths, C. L. (2011). South African pelagic goose barnacles (Cirripedia, Thoracica): Substratum preferences and influence of plastic debris on abundance and distribution. *Crustaceana*, *84*(5/6), 635-649. doi:10.1163/001121611X574290

Xin, Z., Tsuda, T., & Doi, H. (2017). Evaluating the Effects of Air Pollution from a Plastic Recycling Facility on the Health of Nearby Residents. *Acta Medica Okayama*, *71*(3), 209-217. doi:10.18926/AMO/55203

Yoshida, S., Hiraga, K., Takehana, T., Taniguchi, I., Yamaji, H., Maeda, Y., Toyohara, K., Miyamoto, K., Kimura, Y,, Oda, K. (2016). A bacterium that degrades and assimilates poly(ethylene terephthalate). *Science, 351*(6278), 1196–1199.

Yoshida, S., Hiraga, K., Takehana, T., Taniguchi, I., Yamaji, H., Maeda, Y., Toyohara, K., Miyamoto, K., Kimura, Y,, Oda, K. (2016). Supplemental materials for: A bacterium that degrades and assimilates poly(ethylene terephthalate). *Science, 351*(6278), 1–38.

Zhang, C., Chen, X., Wang, J., & Tan, L. (2017). Toxic effects of microplastic on marine microalgae *Skeletonema costatum*: Interactions between microplastic and algae. *Environmental pollution, 220,* 1282-1288.

Zhang, H., Wen, Z.G. (2013). The consumption and recycling collection system of PET bottles: A case study of Beijing, China. *Waste Management, 34*(6), 987–998.

Supplemental Materials

Sequencing Spectra

Primer sequences are shown here. The primers and codon-optimized gene were ordered from Eurofins Scientific. Sequencing Spectra follow.

PETase-5'
GGGCATATGAACTTTCCGCGGGCATCTCGC
PETase-3'
GGGGGATCCTTAGCAGTTGGCTGTGCGAAAGTC
PETase 5' NcoI
GGGCCATGGGGAACTTTCCGCGGGCATCTCGC
PETase 3' no stop
GGGGGATCCGCAGTTGGCTGTGCGAAAGTC
PETaseDelNdeI
GGGCATATGGGGCAGACCAACCCGTATGCCCG

Table S1: List of primers used on PETase sequence for confirmation of correct insertion, preparation of stocks for sequencing, screening of transformed colonies, and addition of endonuclease sites.

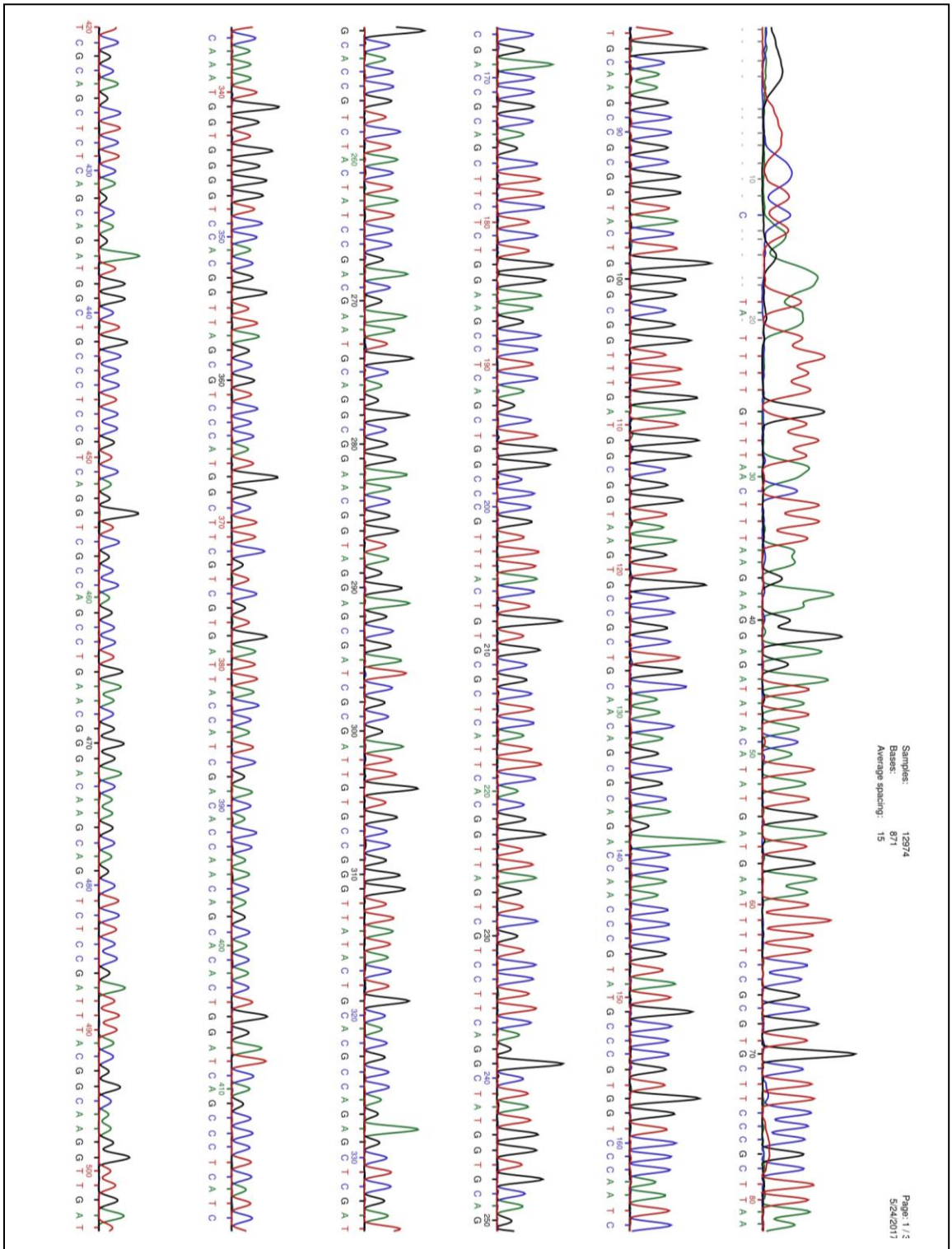

Figure S1: Absorbance spectra of pET3a PETase sequencing.

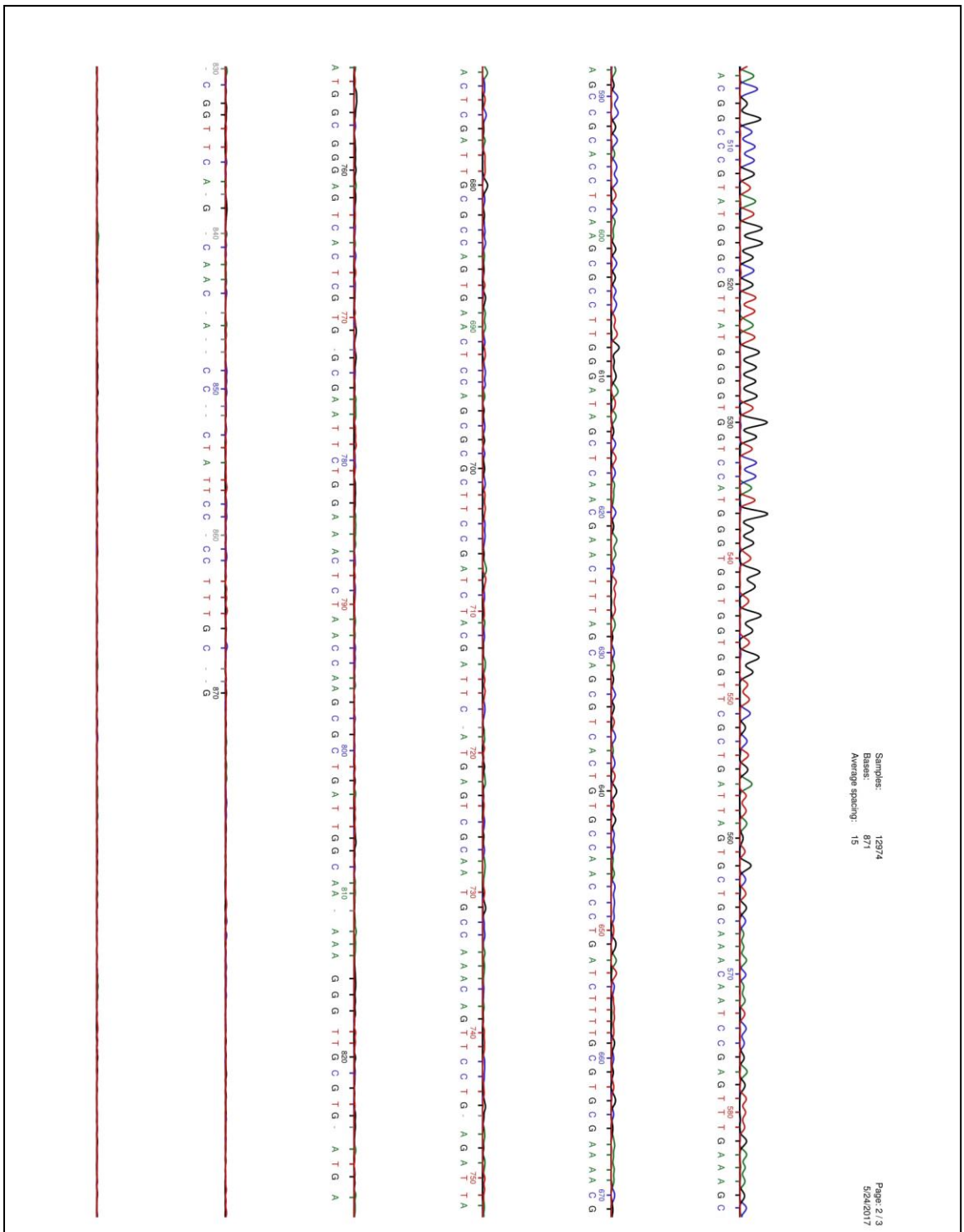

Figure S1 Cont.: Absorbance spectra of pET3a PETase sequencing.

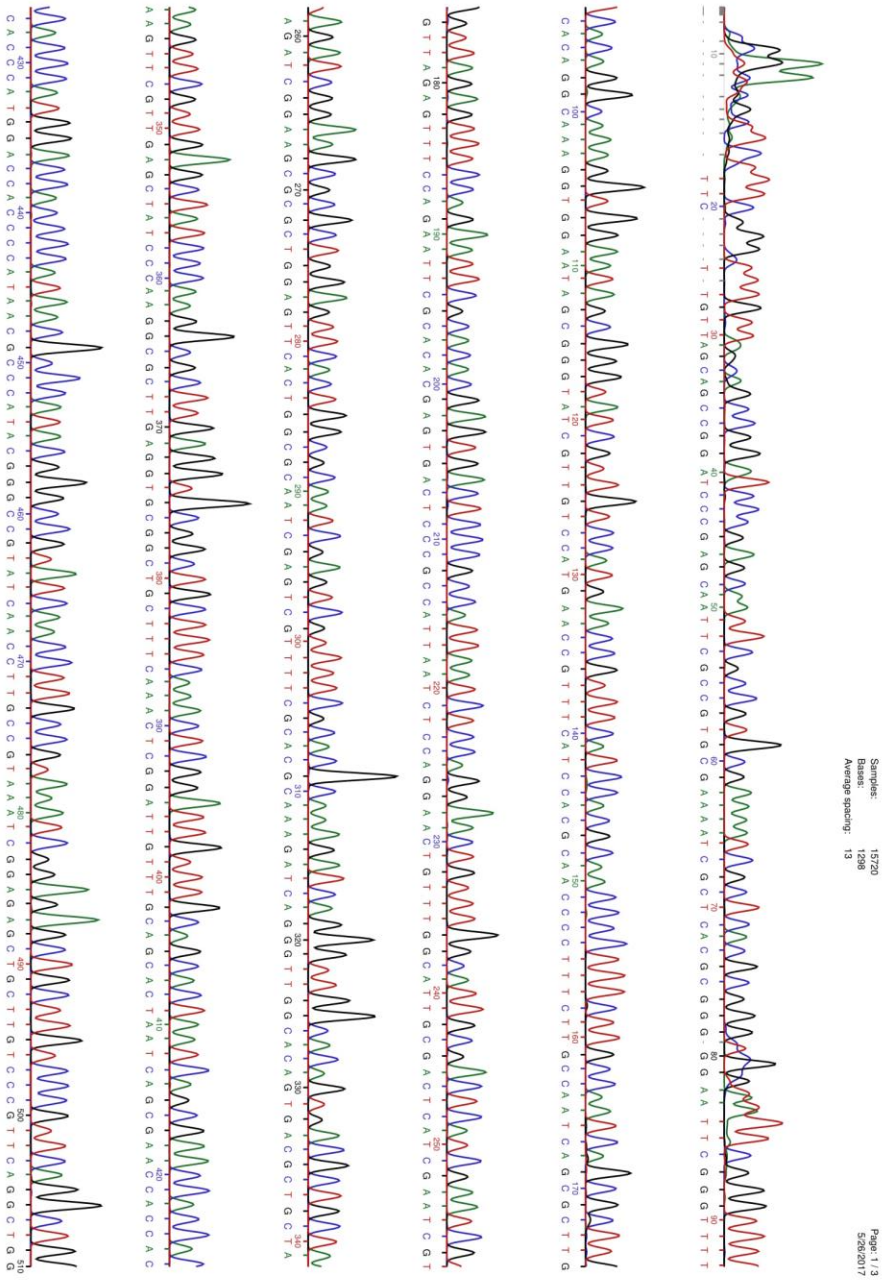

Figure S2: Absorbance spectra of pET3a PETase sequencing from reverse complement.

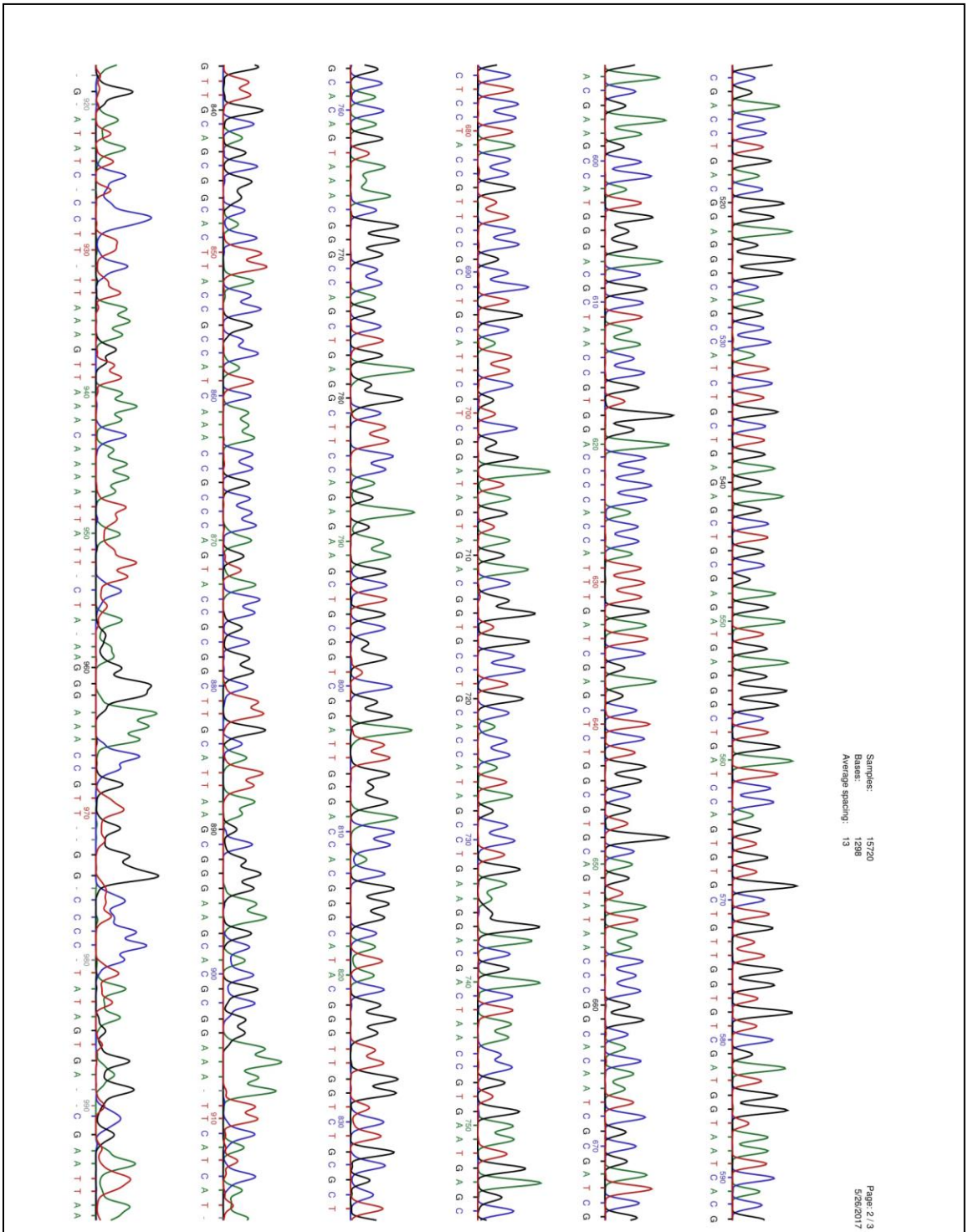

Figure S2 Cont.: Absorbance spectra of pET3a PETase sequencing from reverse complement.

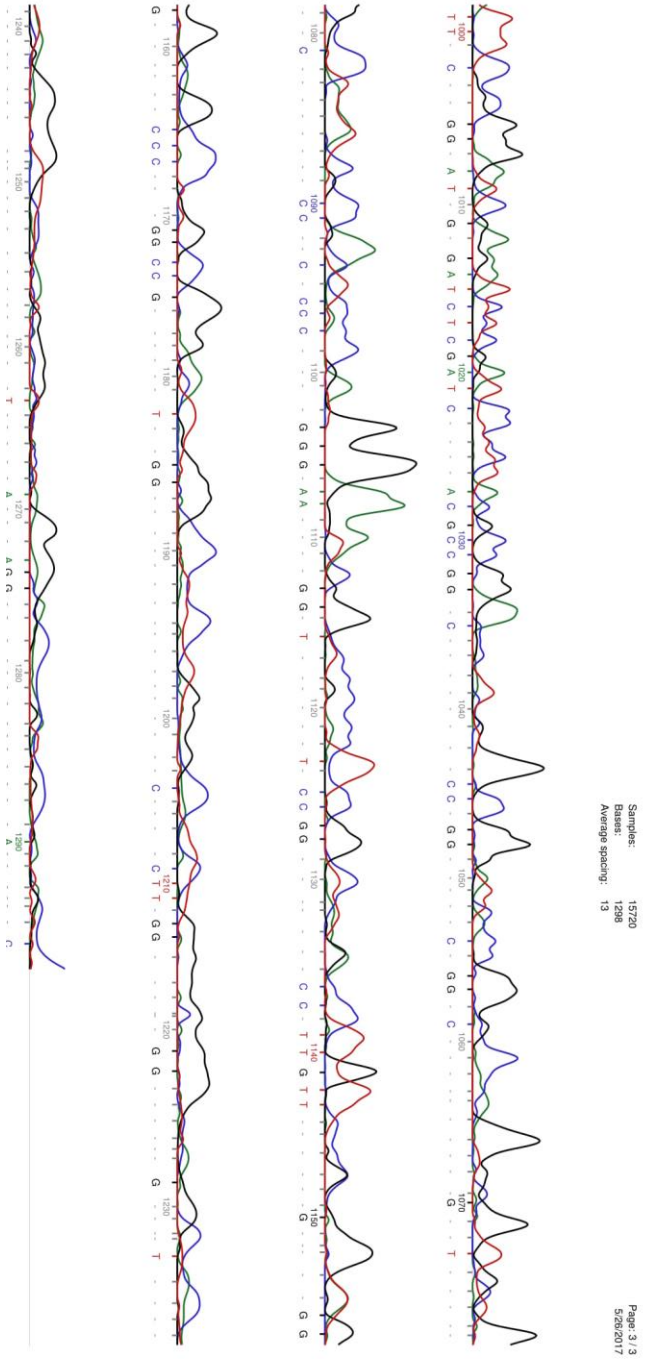

Figure S2 Cont.: Absorbance spectra of pET3a PETase sequencing from reverse complement.

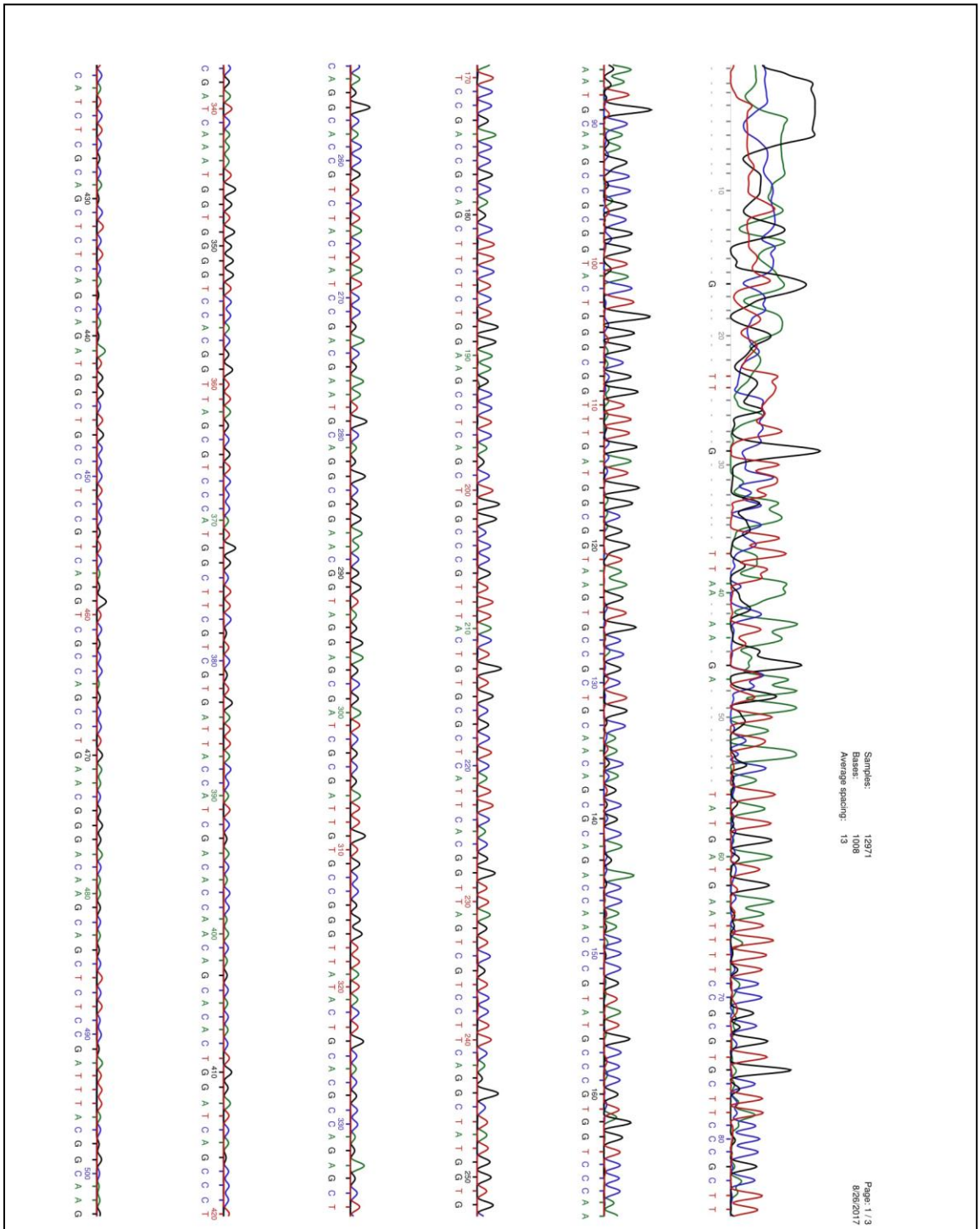

Figure S3: Absorbance spectra of pET14 PETase sequencing.

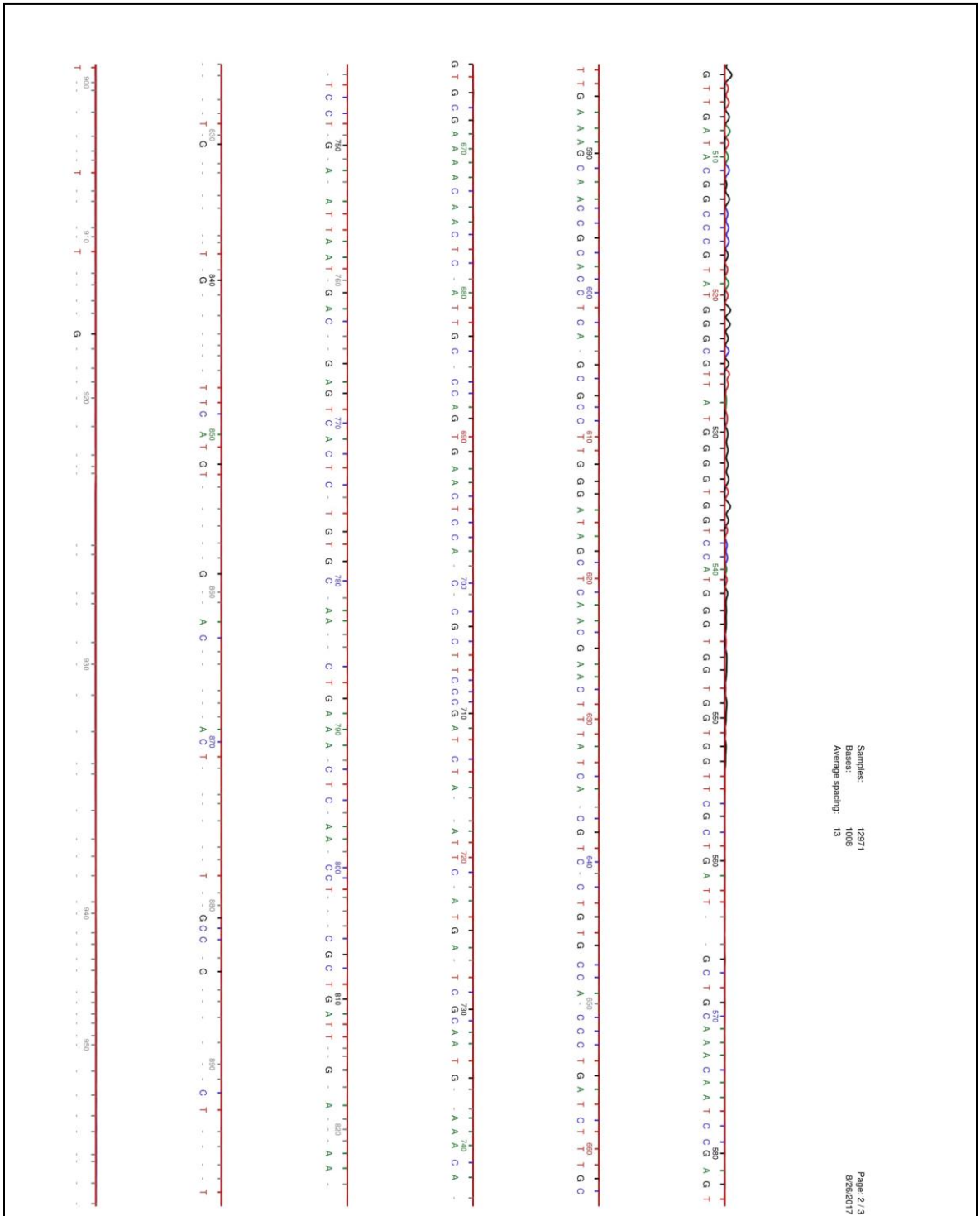

Figure S3 Cont.: Absorbance spectra of pET14 PETase sequencing.

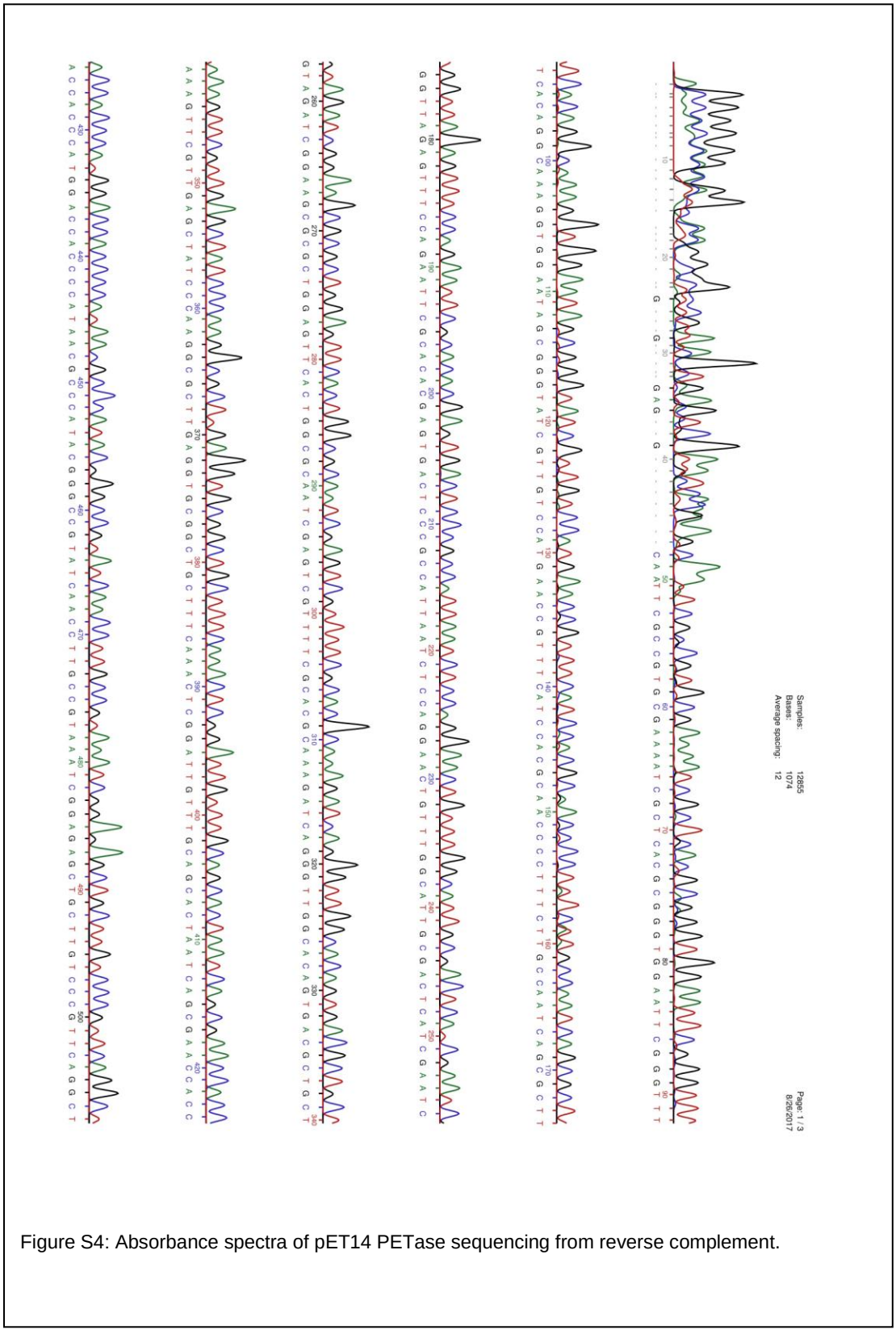

Figure S4: Absorbance spectra of pET14 PETase sequencing from reverse complement.

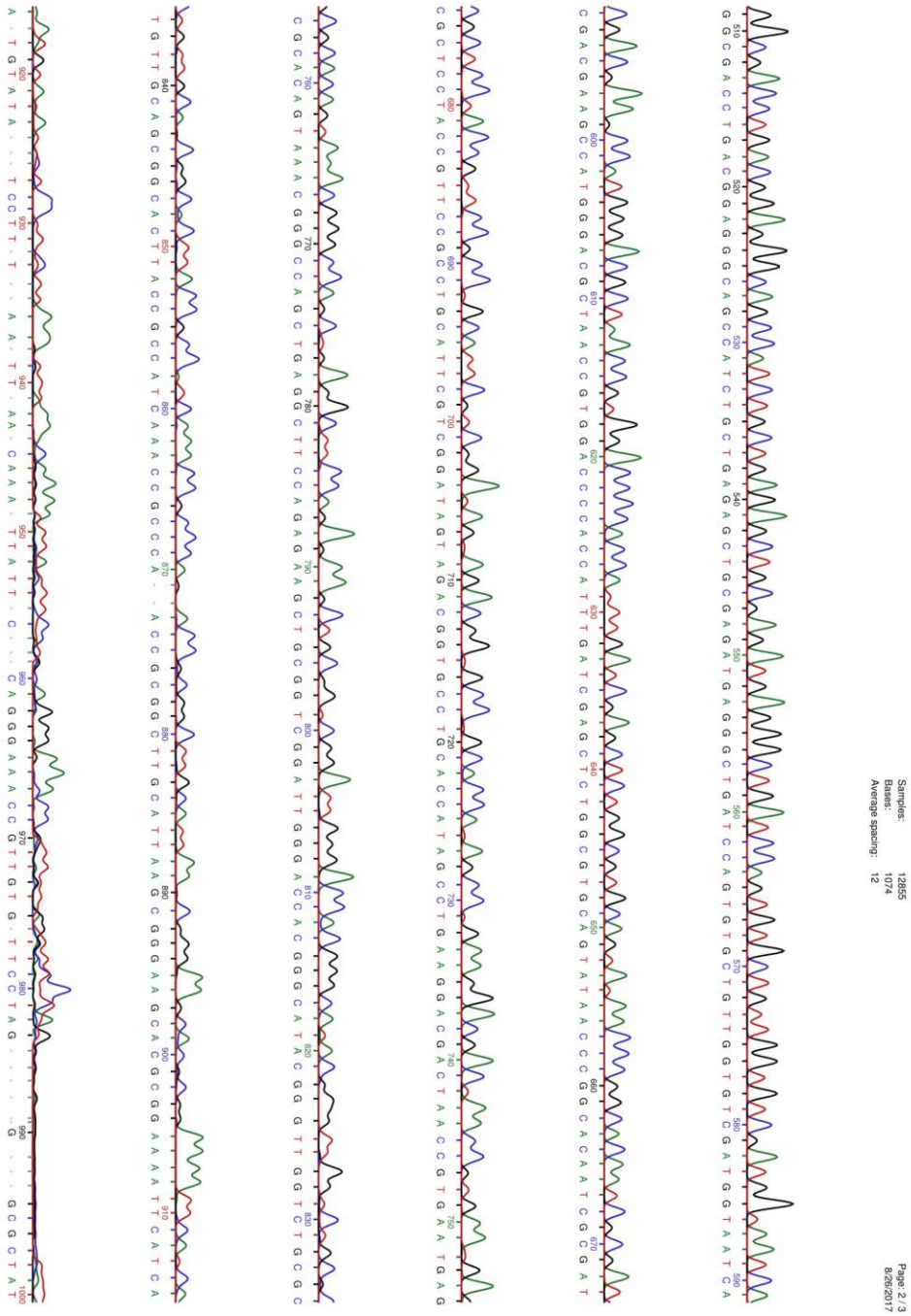

Figure S4 Cont.: Absorbence spectra of pET14 PETase sequencing from reverse complement.

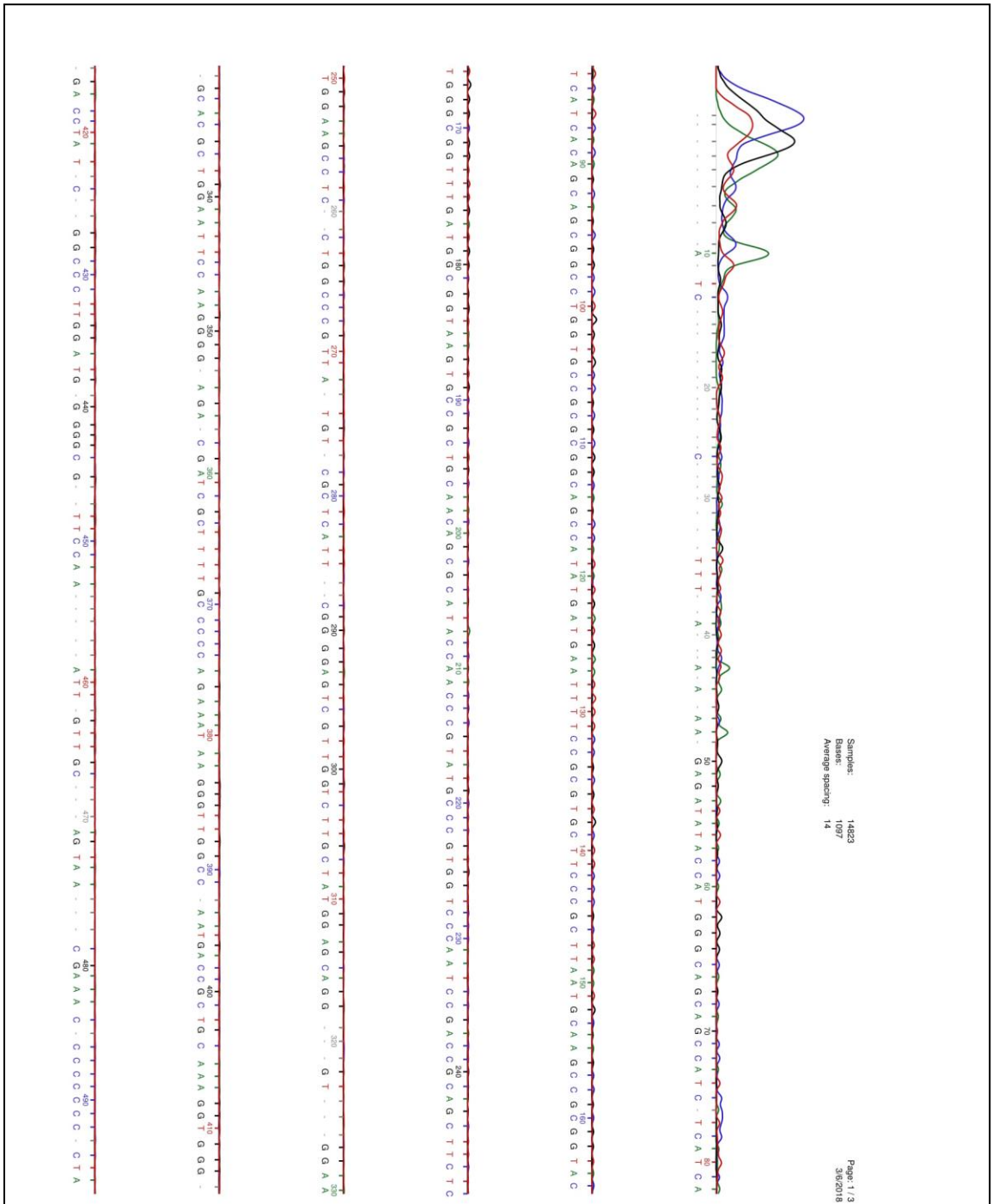

Figure S5: Absorbance spectra of pET28 PETase sequencing.

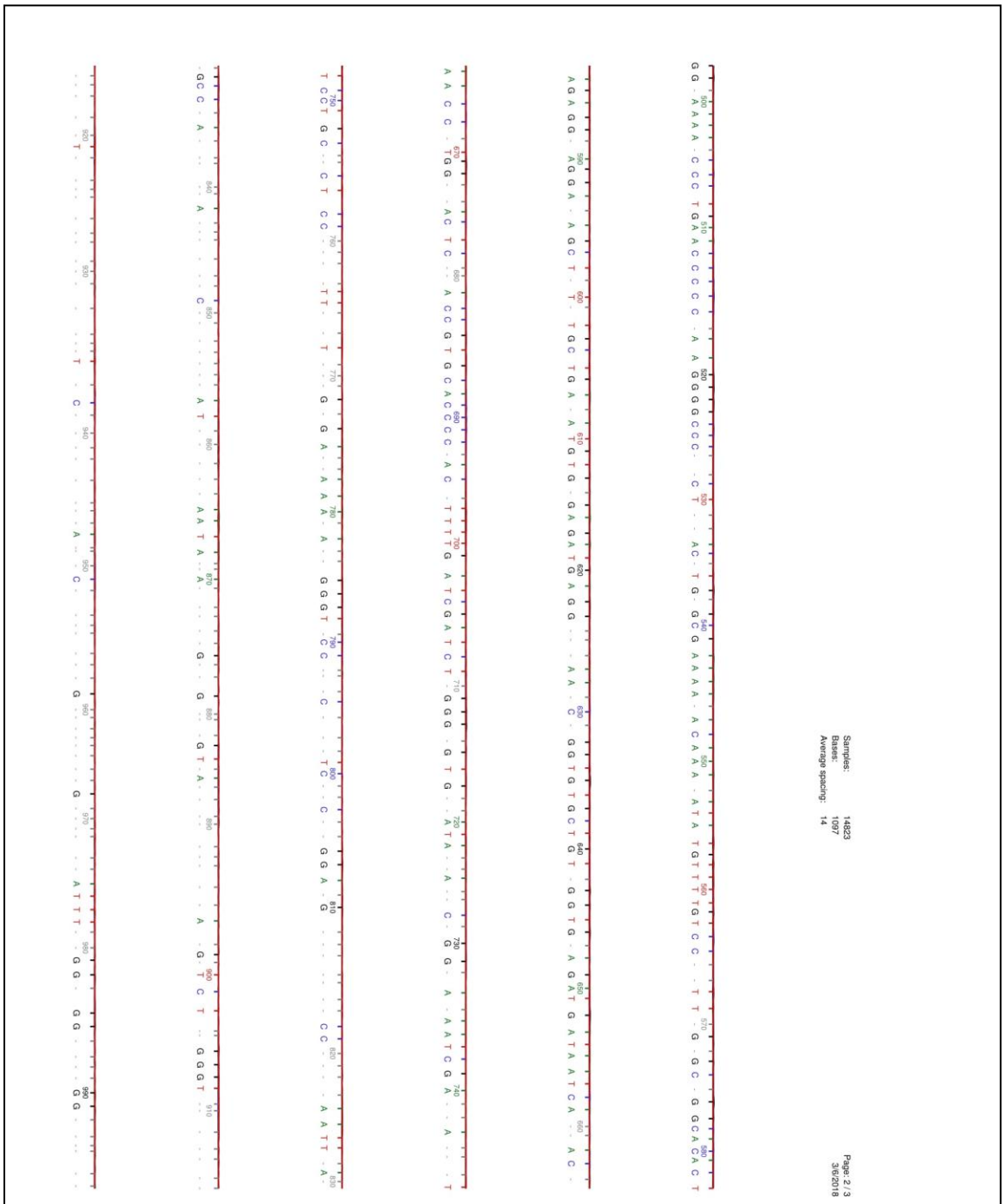

Figure S5 Cont.: Absorbance spectra of pET28 PETase sequencing.

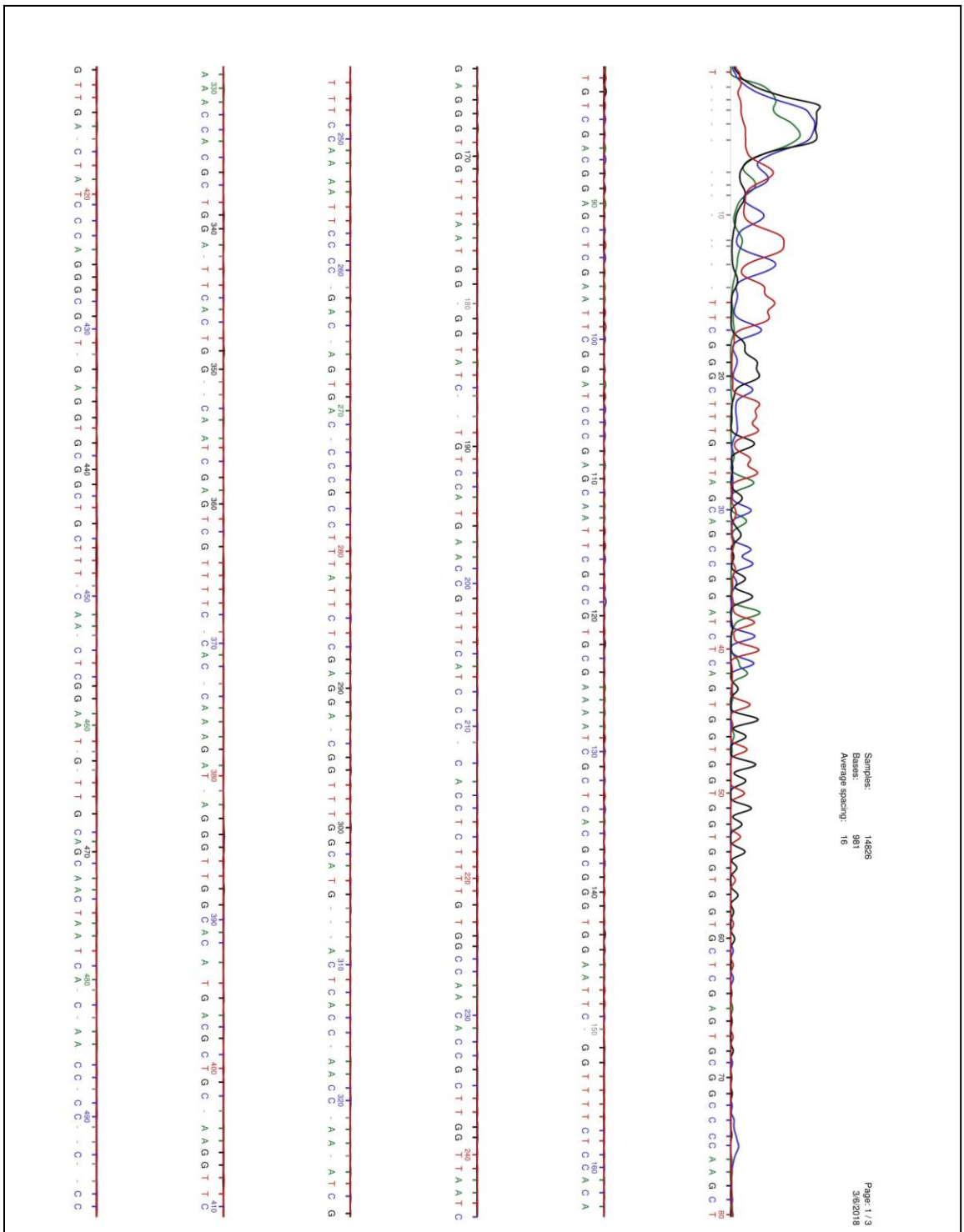

Figure S6: Absorbance spectra of pET28 PETase sequencing from reverse complement.

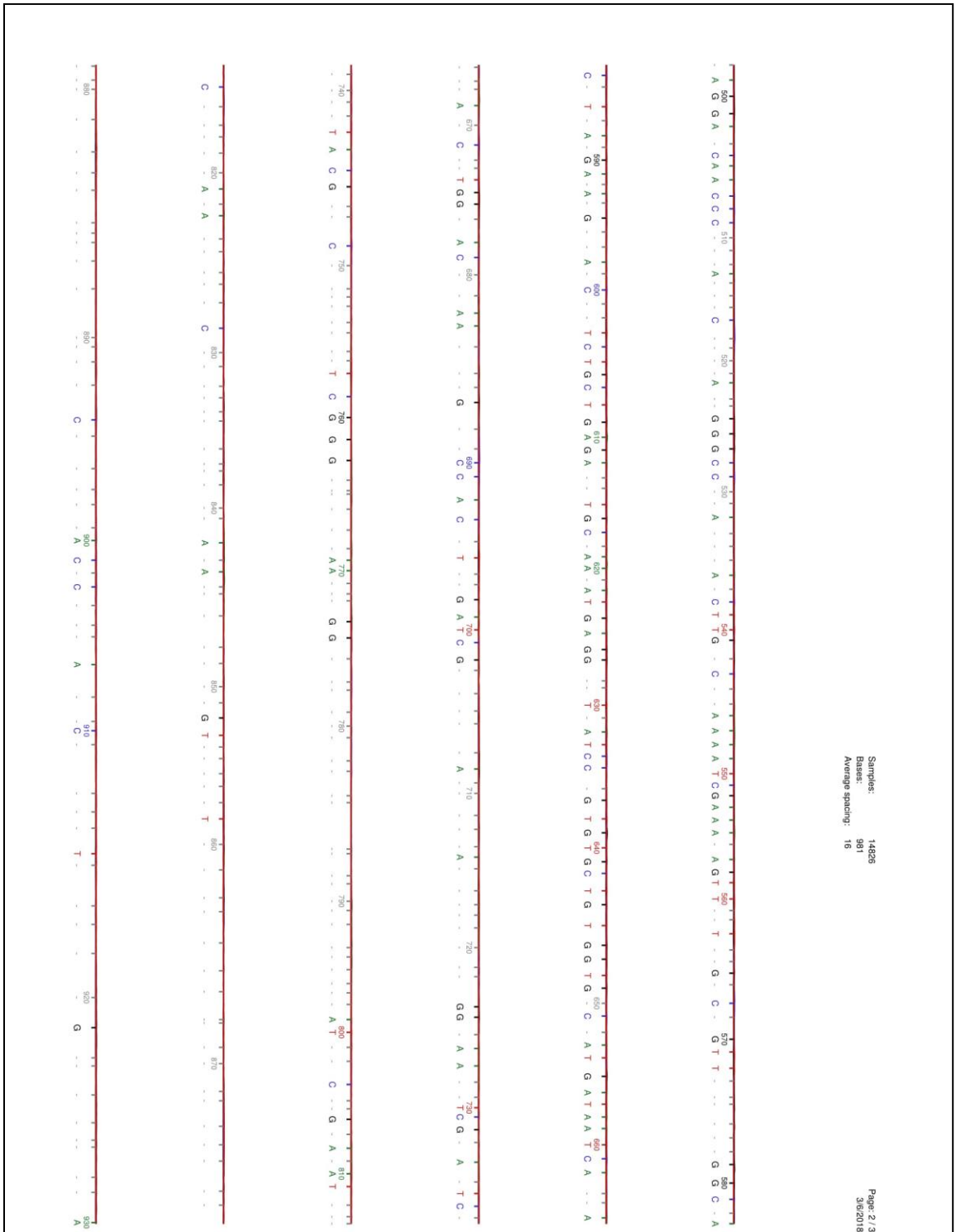

Figure S6 Cont.: Absorbance spectra of pET28 PETase sequencing from reverse complement.

Gel Images

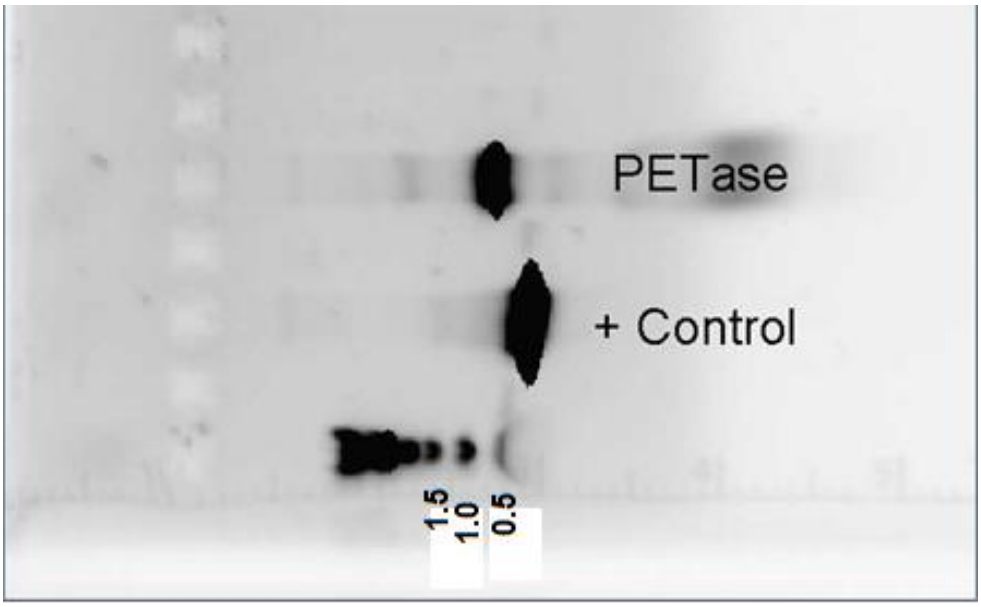

Figure S7: The PETase gene after PCR. The ladder verifies the expected size of the gene, roughly 800-900 bases, considering the primers add Nde1-BamH1 sites to the 5' and 3' ends respectively.

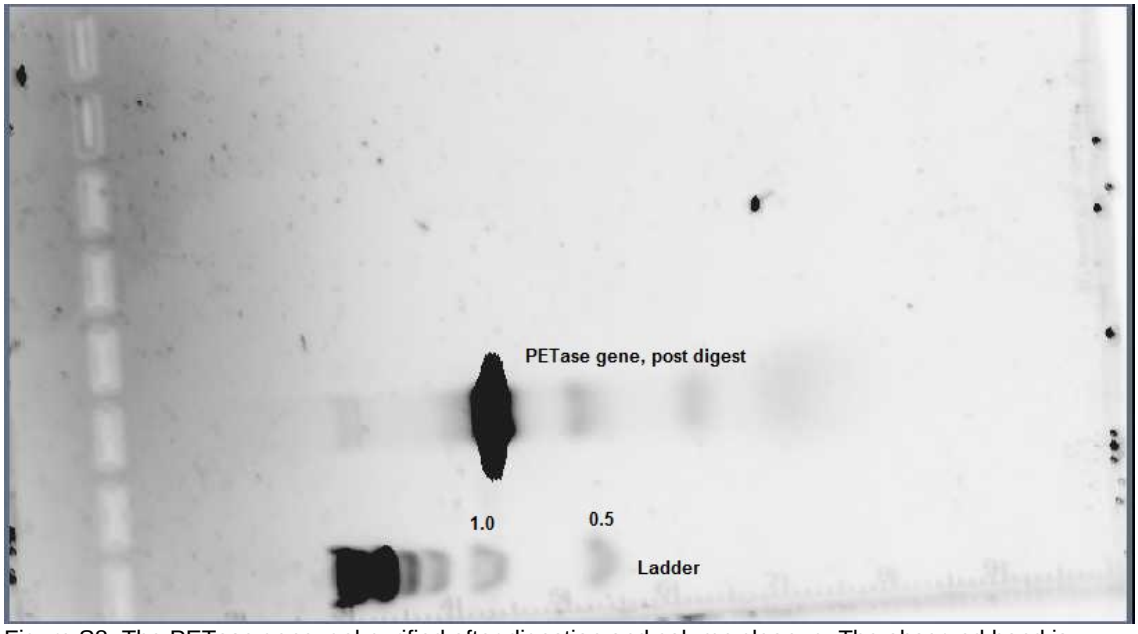

Figure S8: The PETase gene, gel purified after digestion and column cleanup. The observed band is consistent with the 800-900 base size of PETase plus the endonuclease sites, which add about 20 nucleotides..

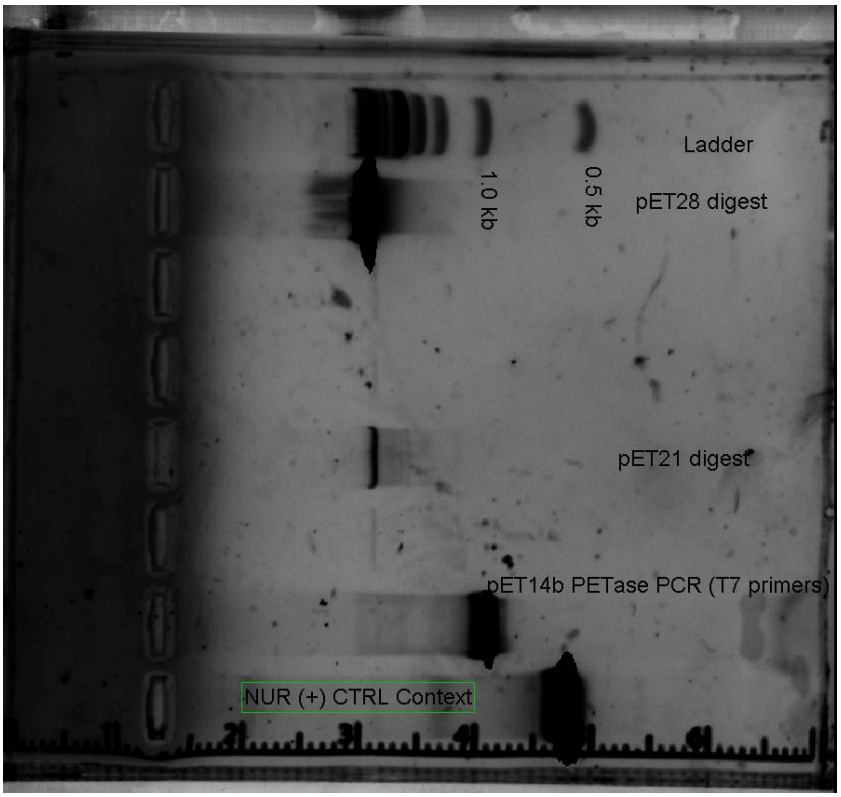

Figure S9: Gel purification of digested pET28 and pET21 plasmids. Digestions were with Nde1-BamH1

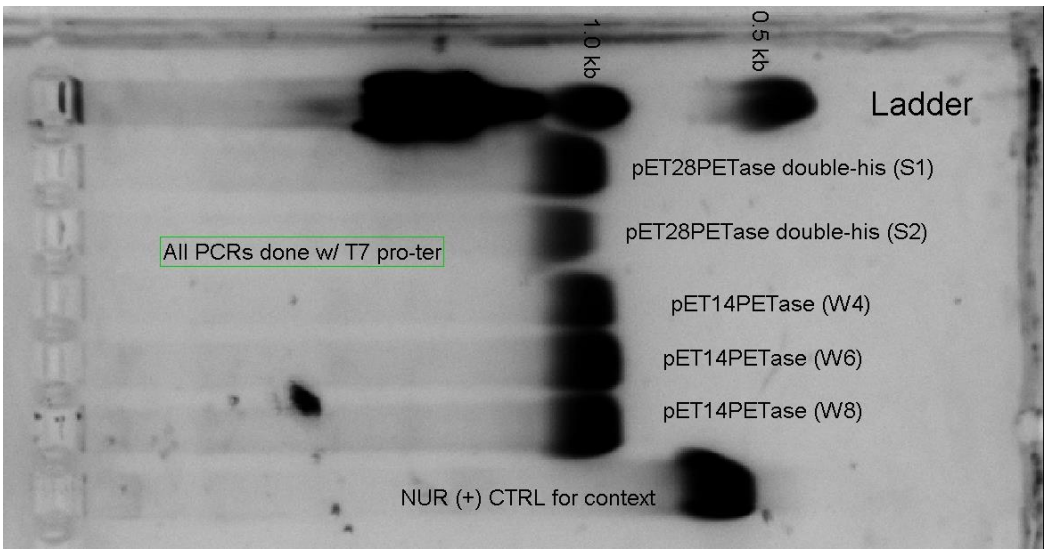

Figure S10: The expected weight of the pET28 PETase is shown in relation with three instances of the pET14 PETase.

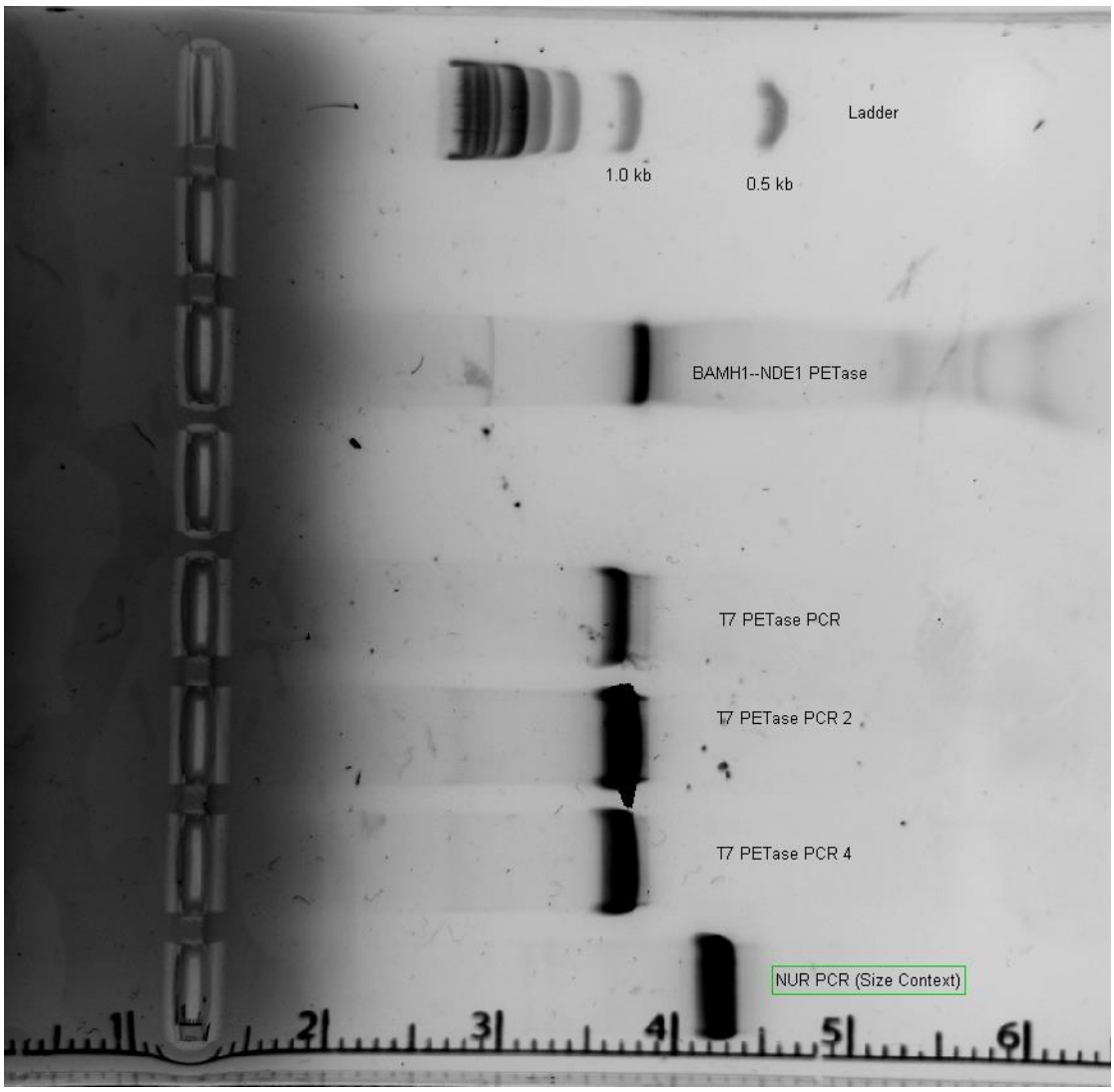

Figure S11: Gel Purification of digested PETase gene with modified 3' (stop codon removed). This allows the translation to continue through onto the plasmid. In our case, we used this method to add a His-tag.

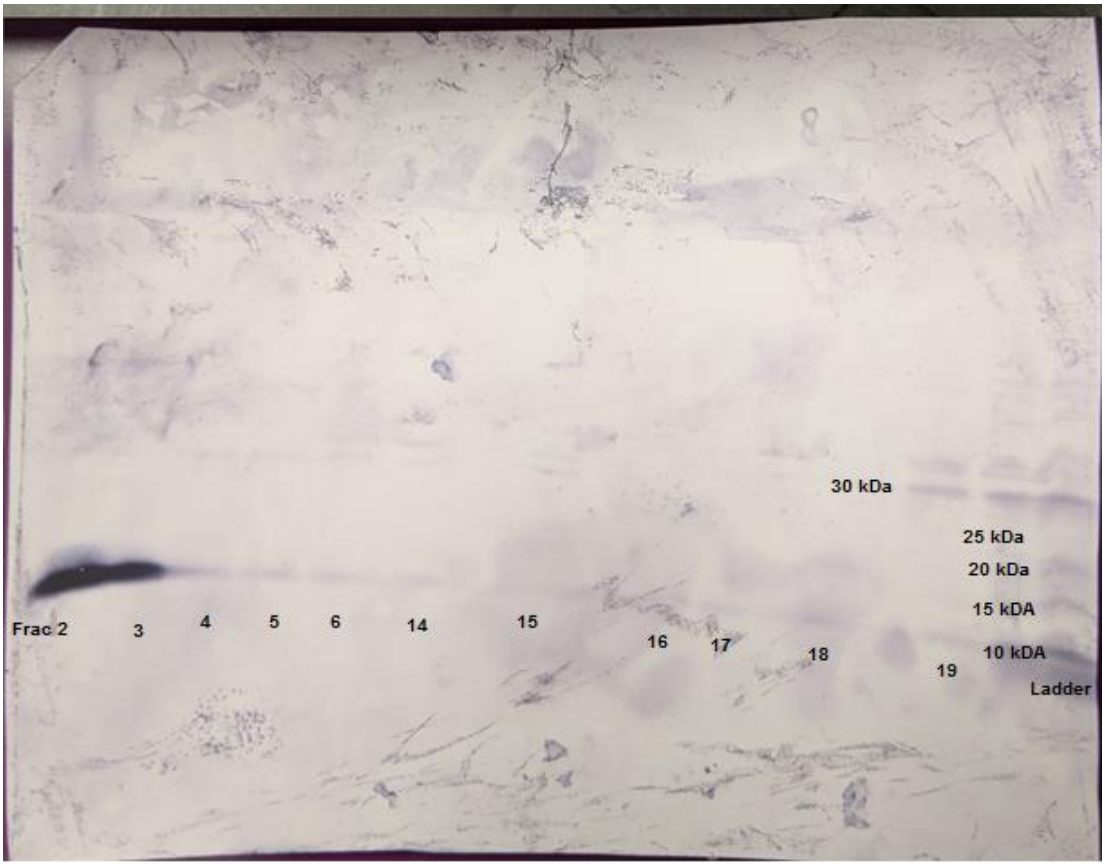

Figure S12: Western blot shows a small amount of protein may have been eluted in fraction 19, The large band of small molecular weight in the flowthrough, suggests that the sample was degraded by proteolysis. Also, the antibody concentration may have been too low to detect the protein in the fractions. Primary antibody: 6x-His Tag Monoclonal Antibody (mouse IgG). GeneTex, catalog # GTX15149. Secondary antibody: Goat anti-Mouse IgG Secondary Antibody. GeneTex catalog # GTX213111-04 (GeneTex, 2013). Blocking agent: TBST with 0.05g/mL nonfat dry milk. Visualization: 0.5x diluted StrepTactin-AP conjugate. Membrane: PVDF